September 2003

Analysis of lateral flow biodetectors: competitive format

Shizhi Qian
University of Pennsylvania

Haim H. Bau
University of Pennsylvania, bau@seas.upenn.edu

Postprint version. Published in *Analytical Biochemistry* , Volume 326, Issue 2, March 2004, pages 211-224.
Publisher URL: http://dx.doi.org/10.1016/j.ab.2003.12.019

Analysis of lateral flow biodetectors: competitive format

Abstract
Lateral flow (LF) biodetectors facilitate low-cost, rapid identification of various analytes. The LF cell consists of a porous membrane containing immobilized ligands at various locations. Through the action of capillary forces, a mixture of sample and reporter particles is transported to the ligand sites, where the target analytes and the reporters bind to the immobilized ligand. The concentration of the reporters is measured with a scanner. A mathematical model for two different competitive assays is constructed and used to study the performance of LF devices under various operating conditions. The model predicts the signal magnitude as a function of target analyte, reporter, and ligand concentrations, reaction rate constants, and flow rate. The predictions are compared and qualitatively agree with experimental data. The model provides insights into various experimental observations. Furthermore, the model can be used to optimize the performance of LF devices and to inexpensively and rapidly test the system under various operating conditions.

Keywords
lateral flow test, point of care testing, immunoassay test strips, lateral flow immunoassay, competitive format

Comments
Postprint version. Published in *Analytical Biochemistry* , Volume 326, Issue 2, March 2004, pages 211-224.
Publisher URL: http://dx.doi.org/10.1016/j.ab.2003.12.019

Qian S., and Bau, H., H., 2004, Analysis of Lateral Flow Bio-detectors: Competitive Format, Analytical Biochemistry 326, 211–224

Analysis of Lateral Flow Bio-detectors: Competitive Format

Shizhi Qian and Haim H. Bau*
Department of Mechanical Engineering and Applied Mechanics,
University of Pennsylvania
Philadelphia, PA 19104-6315

ABSTRACT

Lateral Flow (LF) bio-detectors facilitate low-cost, rapid identification of various analytes. The LF cell consists of a porous membrane containing immobilized ligands at various locations. Through the action of capillary forces, a mixture of sample and reporter particles is transported to the ligand sites, where the target analytes and the reporters bind to the immobilized ligand. The concentration of the reporters is measured with a scanner. A mathematical model for two different competitive assays is constructed and used to study the performance of LF devices under various operating conditions. The model predicts the signal magnitude as a function of target analyte, reporter, and ligand concentrations, as well as reaction rate constants and flow rate. The predictions are compared and qualitatively agree with experimental data. The model provides insights into various experimental observations. Furthermore, the model can be used to optimize the performance of LF devices and to inexpensively and rapidly test the system under various operating conditions.

Key words: lateral flow test, point of care testing, immunoassay test strips, lateral flow immunoassay, competitive format

* All correspondence should be addressed to this author, bau@seas.upenn.edu

1. Introduction

In recent years, there has been a growing interest in developing low-cost techniques for inexpensive, rapid diagnosis of analytes. The Lateral Flow (LF) immunoassay is a popular diagnostic tool because it eliminates the need for trained personnel and expensive equipment.[1-15] Briefly, the LF cell consists of a porous membrane or strip often made out of nitrocellulose. Various antibodies and/or oligonucleotides, to which we refer collectively as ligands, are immobilized at predetermined locations (capture zones) along the porous membrane. A sample containing target analytes is mixed with a buffer solution and pre-engineered reporters such as colloidal gold, carbon black, dyed polystyrene, phosphor, and dye-encapsulating liposomes. The mixture then is introduced into the membrane by capillary forces. As the mixture flows along the capture zones, the analytes and/or the reporters bind to the immobilized ligands. Two common formats are the sandwich and the competitive assays.

When the sandwich assay is used, some of the target analytes bind to the reporters and some remain free in the solution. When the mixture passes through the capture zone, both unbound analytes and bound analytes bind to the ligands. After some time, the LF strip is scanned and the concentration of the reporters is measured as a function of location. An elevated concentration in the capture zone indicates the presence of the target analytes. The sandwich assay has the advantage that the presence of a signal indicates the presence of target analytes. Unfortunately, this is not true at high target analyte concentrations. Once the target analyte concentration exceeds a certain critical value, further increases in the target analyte concentration lead to a reduction in the signal[16]. Another disadvantage of the sandwich assay is that the target analytes must be able to bind simultaneously to both the reporter and the immobilized ligand. This feat typically cannot be accomplished with small analyte molecules that may have a single

antigenic determinant. Additionally, steric hindrance may prevent simultaneous binding of the analyte to both the reporter and the ligand. For an analysis of LF bio detectors operating with sandwich assays, see Qian and Bau.[16]

Given the limitations of the sandwich assays listed above, when the target analytes consist of small molecules, competitive assays are often preferred. In the competitive format, the reporter can bind directly to the immobilized ligands; they do not require the analyte to provide the linkage between the reporter and the ligand as in the sandwich assay. In different manifestations of the competitive format, the target analytes can bind either to the reporter particles[15, 17] or to the immobilized ligands[18-20]. In either case, the presence of target analytes interferes with the binding of the reporter to the test ligands. Thus, when the solution does not contain any target analytes, one would observe a signal at the capture (test) strip. A diminishing or non-existent signal indicates the presence of target analytes in the sample. In order to verify that the device does, indeed, function, a control line is often added to provide a control signal. The control line consists of an immobilized (control) ligand that can bind to the reporter but not to the target analytes.

In the first format of competitive assay, the target analytes bind to the ligands and block the ligands from binding to the reporters.[18-20] For example, Ho et al.[18] use liposome particles conjugated with aflatoxin B_1 (AFB_1) to detect AFB_1. AFB_1 antibody is immobilized at the capture zone, where competition occurs between the AFB_1-conjugated liposomes and analytes (AFB_1) in the sample for binding sites on the AFB_1 antibody.

In the second format of competitive assay, the target analytes bind to the reporters and block these reporters from binding to the immobilized ligand. This format is used, for example, by Esch et al.[15] to detect water-borne cryptosporidium parvum oocysts, and by Niedbala et al.[17]

to detect drugs of abuse. Esch et al.[15] immobilize oligonucleotides (compatible with amplicons produced from C. parvum mRNA) and biotin to the surface of dye-entrapping liposomes. The capture (test) ligand and the control ligand consist, respectively, of antisense oligonucleotides and antibiotin antibodies. In the experiments by Niedbala et al.[17], the test ligands consisted of BSA labeled with the drug hapten and the control line consisted of anti-mouse IgG.

LF immunoassay technology is widely used in hospitals, laboratory medicine, life science research, and the monitoring of water and food quality. Currently, it appears that the developers of LF reactors rely mostly on empirical data to design their devices. Although experiments are indispensable to verify that a device meets expectations, it would be useful to have a predictive tool that allows simulation and optimization of a device, and limit laboratory experiments to the most promising cases. In this paper, we describe such a simple model for a LF competitive assay.

2. MATHEMATICAL MODEL

We consider a lateral flow (LF) reactor that consists of a flat, porous membrane. [9-15, 17-24] The LF cell is schematically diagrammed in Fig. 1. A sample containing target analytes (A), reporters (P), and buffer solution is introduced in a reservoir that is in contact with a dry porous membrane (typically made of nitrocellulose). The solution flows through the membrane by capillary action. Various (test) ligands (R_T) are immobilized typically in strip transverse to the flow direction. Additionally, the membrane is equipped with a control line to which reporters (but no target analytes) can bind. We denote the immobilized (control) ligand in the control line as R_C. For simplicity, we consider a single target analyte. The analysis can be readily extended to account for multiple target analytes.

Two different competitive formats are often used. In the first format, both the reporters (*P*) and the target analyte (*A*) can bind to the immobilized ligand to form, respectively, the complexes R_TP and R_TA.[18-20] Once the ligand has formed the complex R_TA, it is no longer available to bind with a reporter. Only the reporters (but not the target analyte) can bind to the control line to form the complex R_CP. Thus the target analytes compete with the reporters for binding sites. We refer to this format as **RPA** to indicate that both reporter particles (**P**) and target analyte (**A**) can bind to the test ligand (**R**).

In the second format, the reporter particles can bind with either the target analyte or the test ligand (R_T)[15, 17]. Once the target analyte (*A*) binds to the reporter (*P*) to form the complex *PA*, the reporter cannot bind to the ligand R_T. It can, however, still bind to the control line to form the complex R_CPA. The free reporters (*P*), but not the complex *PA*, can bind to the immobilized test ligand (R_T) at the capture zone to form the complex R_TP. The free reporters (*P*) can also bind to the immobilized ligand (R_C) at the control line to form the complex R_CP. The target analytes can bind neither to the test ligand nor to the control ligand. We refer to this format as **RPNA** to indicate that the reporter particles (**P**) but **N**ot the target analyte (**A**) can bind to the test ligand (**R**).

2.1 **RPA** Format: both target analytes and reporters bind to the test ligand

A solution containing the target analytes (*A*) with initial concentration [A_0], reporters (*P*) with initial concentration [P_0], and buffer solution flows up the membrane to the capture zone (test section). Typically, the porous membrane is narrow and thin. The sample moves as a slug with a distinct liquid-air interface at average velocity *U*. The ligands at the test site are immobilized uniformly in the strip $x_{T1}<x<x_{T2}$. Consequently, we need to consider only one space

dimension (x) that is aligned along the membrane's length. To the first approximation, we assume that the captured reporters do not significantly affect the porous membrane's permeability to liquid flow.

We use square brackets ([]) to denote concentrations. The concentrations of the various reagents are functions of both space and time. For example, $[A](x,t)$ is the concentration of the target analyte at location x and time t. In the capture (test) zone, the target analytes (A) and the reporters (P) bind to the immobilized ligands to form, respectively, the complexes R_TP ($P+R_T \leftrightarrows R_TP$) and R_TA ($A+R_T \leftrightarrows R_TA$). We assume reversible interactions with 1:1 kinetics. Once a ligand has formed the complex R_TA, it is no longer available to bind with a reporter.

The rate of formation (F_{RTA}) of the ligand-analyte complex (R_TA) in the capture (test) zone is proportional to the product of the free analytes ([A]) and unbound (free) ligand:

$$F_{RTA} = k_{a1}[A]([R_{T0}] - [R_T A] - [R_T P]) - k_{d1}[R_T A]. \quad (1)$$

Similarly, the rate of formation (F_{RTP}) of the ligand-reporter complex (R_TP) at the capture (test) site is:

$$F_{RTP} = k_{a2}[P]([R_{T0}] - [R_T A] - [R_T P]) - k_{d2}[R_T P]. \quad (2)$$

In the above, $[R_{T0}]$ is the initial concentration of the test ligand (prior to the binding events). $[R_{T0}]$-$[R_TA]$-$[R_TP]$ is the instantaneous concentration of free ligands that is available for binding. k_{ai} and k_{di} are, respectively, the appropriate association and dissociation rate constants.

After going through the capture (test) zone, the mixture passes through the control line that is located at $x_{C1}<x<x_{C2}$. At the control site, the reporters interact with the immobilized ligand (R_C) to form the complex R_CP ($P+R_C \leftrightarrows R_CP$). The rate of formation (F_{RCP}) of the ligand-reporter complex (R_CP) is:

$$F_{RCP} = k_{a3}[P]([R_{C0}] - [R_C P]) - k_{d3}[R_C P]. \quad (3)$$

In the above, $[R_{C0}]$ and $[R_{C0}]$-$[R_CP]$ are, respectively, the initial ligand concentration and the instantaneous concentration of the (free) ligand available for binding at the control line. The complex PA does not bind to the control ligand.

The concentrations of the free target analyte ($[A](x, t)$), the free particle reporters ($[P](x,t)$), the ligand-analyte complex at the test site ($[R_TA](x,t)$, the ligand-reporter complex at the test site ($[R_TP]$), and the ligand-reporter complex at the control site ($[R_CP]$) are described, respectively, by the convection-diffusion-reaction equations:

$$\frac{\partial [A]}{\partial t} = D_A \frac{\partial^2 [A]}{\partial x^2} - U \frac{\partial [A]}{\partial x} - F_{RTA}, \tag{4}$$

$$\frac{\partial [P]}{\partial t} = D_P \frac{\partial^2 [P]}{\partial x^2} - U \frac{\partial [P]}{\partial x} - (F_{RTP} + F_{RCP}), \tag{5}$$

$$\frac{\partial [R_T A]}{\partial t} = F_{RTA}, \tag{6}$$

$$\frac{\partial [R_T P]}{\partial t} = F_{RTP}, \tag{7}$$

and

$$\frac{\partial [R_C P]}{\partial t} = F_{RCP}. \tag{8}$$

In the above, we assume that the cross-section averaged fluid velocity is obtained from experimental data (U~0.2 mm/s). Time-dependent velocity can be readily incorporated into the model. D_A and D_P are, respectively, the molecular diffusion coefficients of the analyte and the reporters. We assume that the analyte's molecular mass is ~47kg/mol and the equivalent molecular mass of the reporters is 7000kg/mol. Accordingly, we use the Stokes-Einstein equation to estimate $D_A \sim 1.0\times10^{-10}$ m^2/s and $D_P \sim 2.0\times10^{-11}$ m^2/s. The values of the diffusion

coefficients affect the process dynamics but not the equilibrium states. F_{RTA} and F_{RTP} occur and $[R_TA]$ and $[R_TP]$ exist only in the capture (test) zone and are equal to zero elsewhere. Similarly, F_{RCP} occurs and $[R_CP]$ exists only at the control site and are equal to zero elsewhere.

We consider the case when the reporters are premixed with the sample prior to their introduction into the membrane. Specifically, a sample containing concentrations $[A_0]$ and $[P_0]$ of the target analyte and reporters is introduced into a chamber that is in contact with the membrane. Thus, at $x=0$,

$$[A](0,t)=A_0 \text{ and } [P](0,t)=P_0. \tag{9}$$

At the membrane exit ($x=L$), we specify the customary outflow conditions:

$$\frac{\partial [A](L,t)}{\partial x} = \frac{\partial [P](L,t)}{\partial x} = 0\,. \tag{10}$$

Given the smallness of the diffusion coefficients, the outflow boundary conditions do not affect upstream events and do not have any significant effect on the model's predictions.

The initial conditions are:

$$[A](x,0)=[P](x,0)=[R_TA](x,0)=[R_TP](x,0)= [R_CP](x,0)=0. \tag{11}$$

The total reporter concentration is typically detected with a scanner. The scanner measures either the fluorescent or phosphor emission intensity or color intensity. At the capture (test) site, the scanner's signal is proportional to $S_T=[P]+[R_TP]$. At the control site, $S_C=[P]+[R_CP]$. Away from the interaction zones, the scanner's signal is proportional to $S_0=[P]$. We refer to S_0 as the background signal. We define the amplitude $\Delta S_T=S_T-S_0$ and the contrast index $DS_T = \frac{S_T - S_0}{S_0}$. We denote the signal levels (S^0) in the absence of target analyte ($[A_0]=0$) with superscript 0.

Before concluding this section, we consider the simplified special case of the well-mixed capture (test) zone. When the flow rate is relatively high, the various species are nearly uniformly distributed in space ($\frac{\partial}{\partial x} = 0$) and the interaction has little effect on the concentrations of the target analyte and the reporters in the solution. Furthermore, we assume that the interactions have reached an equilibrium state. It is instructive to consider this idealized case since it allows us to derive relatively simple algebraic expressions for the equilibrium concentrations of the test ligand-analyte (R_TA), test ligand-reporter (R_TP), and control ligand-reporter (R_CP) complexes, and gain a few important insights.

At the well-mixed capture (test) site, the equilibrium concentrations of the ligand-reporter (R_TP) and ligand-analyte (R_TA) complexes are, respectively,

$$[R_T P]_E = \frac{k_{a2} k_{d1} [P_0][R_{T0}]}{k_{a1} k_{d2} [A_0] + k_{a2} k_{d1} [P_0] + k_{d1} k_{d2}} \tag{12}$$

and

$$[R_T A]_E = \frac{k_{a1} k_{d2} [A_0][R_{T0}]}{k_{a1} k_{d2} [A_0] + k_{a2} k_{d1} [P_0] + k_{d1} k_{d2}}. \tag{13}$$

In the above, the subscript E indicates equilibrium conditions. Away from the test site, $[R_TP]=[R_TA]=0$.

At the control site, the equilibrium concentration of the ligand- reporter ($[R_CP]$) complex is:

$$[R_C P]_E = \frac{k_{a3} [P_0][R_{C0}]}{k_{a3} [P_0] + k_{d3}} \tag{14}$$

In the well-mixed case, at the capture (test) site, the scanner's signal is proportional to S_T=[P]+[PA]+$[R_TP]_E$=$[P_0]$+$[R_TP]_E$. At the control site, S_C=[P]+[PA]+$[R_CP]_E$=$[P_0]$+$[R_CP]_E$. Away from the interaction zones, the scanner signal is S_0= $[P_0]$. Thus, the contrast index

$$DS_T = \frac{[R_T P]_E}{[P_0]} = \frac{k_{a2}k_{d1}[R_{T0}]}{k_{a1}k_{d2}[A_0] + k_{a2}k_{d1}[P_0] + k_{d1}k_{d2}} \tag{15}$$

and $\Delta S_T = [R_TP]_E$. The signal level S_T-S_0 at the capture (test) zone

$$\Delta S_T \sim \frac{k_{a2}k_{d1}[P_0][R_{T0}]}{k_{a2}k_{d1}[P_0] + k_{d1}k_{d2}} \tag{16}$$

is nearly constant when the target concentration is below the threshold $[A_C]$. When $[A_0]$<<$[A_C]$,

$$[A_C] = \frac{k_{a2}k_{d1}[P_0] + k_{d1}k_{d2}}{k_{a1}k_{d2}}. \tag{17}$$

In other words, target analyte concentrations below the threshold $[A_C]$ will not be detectable. Witness that the magnitude of the threshold depends on the reporter concentration, and can be lowered by decreasing $[P_0]$.

When the target analyte concentration exceeds the threshold ($[A_C]$), the signal's magnitude is inversely proportional to the target analyte's concentration in the sample. When $[A_0]$>> $[A_C]$,

$$\Delta S_T \sim \frac{k_{a2}k_{d1}[P_0][R_{T0}]}{k_{a1}k_{d2}[A_0]}. \tag{18}$$

Next, we examine the effect of the reporter concentration on the signal. When the reporters' concentration ($[P_0]$) is small,

$$\Delta S_T \sim \frac{k_{a2}k_{d1}[R_{T0}]}{k_{a1}k_{d2}[A_0] + k_{d1}k_{d2}}[P_0] \tag{19}$$

increases nearly linearly as the reporter's concentration increases. One should bear in mind, however, that as $[P_0]$ increases so does $[A_C]$. Hence there are tradeoffs between signal intensity and detector sensitivity.

Finally, witness that under equilibrium conditions, the control signal's magnitude is independent of the target analyte concentration (equation 14). Prior to the establishment of equilibrium, however, the control signal increases as the target analyte concentration increases.

2.2 **RPNA** Format: target analytes bind to reporters but not to the test ligand

In this competitive assay format,[15] the target analyte (if present) would bind to a reporter to form the complex *PA*. The target analyte-reporter complex (*PA*) cannot bind to the test ligand R_T. Only free reporters (*P*) can bind to the test ligand (R_T). Both the analyte-reporter complex (*PA*) and the free reporters (*P*) can bind to the immobilized ligand (R_C) at the control site. As was the case with the previous format (section 2.1), as the target analyte concentration increases, the signal level in the capture zone decreases.

In the **RPNA** competitive format, a sample containing, respectively, concentrations $[A_0]$ and $[P_0]$ of the target analytes and reporters is introduced into a chamber that is in contact with the membrane. Since the reporters and target analytes are premixed, the interaction $A+P \leftrightarrows PA$ takes place prior to the solution's entry into the membrane. In other words, the sample entering the membrane consists of free target analytes (*A*), free reporters (*P*), and analyte-reporter complex (*PA*). The concentration of each of the above depends on the residence time and the stirring conditions in the chamber. Since these conditions may vary from one case to another, we consider here just one extreme case. We assume that the mixture of the target analytes and

reporters was allowed sufficient time to equilibrate prior to entering the capture (test) zone. The corresponding equilibrium concentrations are denoted with the subscript *e*:

$$[PA_e] = \frac{[A_0] + [P_0] + \frac{k_{d1}}{k_{a1}} - \sqrt{\left([A_0] + [P_0] + \frac{k_{d1}}{k_{a1}}\right)^2 - 4[A_0][P_0]}}{2} \tag{20}$$

$$[A_e] = [A_0] - [PA_e] \tag{21}$$

and

$$[P_e] = [P_0] - [PA_e]\,. \tag{22}$$

In the above, k_{a1} and k_{d1} are association and dissociation rate constants for the reaction $A+P \leftrightarrows PA$. In the capture (test) zone, reporters bind to the immobilized (test) ligand (R_T) through the reversible interaction ($P+R_T \leftrightarrows R_TP$). At the control site, the analyte-reporter complex (PA) binds to the immobilized (control) ligand (R_C) to form a ligand-analyte-reporter complex R_CPA ($PA+R_C \leftrightarrows R_CPA$). Additionally, free reporters can also bind to the control ligand to form the complex R_CP through the reversible interaction ($P+R_C \leftrightarrows R_CP$).

The rate of formation (F_{PA}) of the analyte-reporter complex (PA) is proportional to the product of the free analyte ([A]) and free reporters ([P]) concentrations:

$$F_{PA} = k_{a1}[A][P] - k_{d1}[PA]\,. \tag{23}$$

Similarly, the rate of formation (F_{RTP}) of the ligand-reporter complex (R_TP) in the capture (test) zone is:

$$F_{RTP} = k_{a2}[P]([R_{T0}] - [R_TP]) - k_{d2}[R_TP]\,. \tag{24}$$

At the control site, the rate of formation (F_{RCPA}) of the ligand-analyte-reporter complex (R_CPA) is:

$$F_{RCPA} = k_{a3}[PA]([R_{C0}] - [R_CPA] - [R_CP]) - k_{d3}[R_CPA]\,, \tag{25}$$

and the rate of formation (F_{RCP}) of the ligand-reporter complex (R_CP) is:

$$F_{RCP} = k_{a4}[P]([R_{C0}]-[R_CPA]-[R_CP]) - k_{d4}[R_CP]. \quad (26)$$

In the above, k_{aj} and k_{dj} are, respectively, the appropriate association and dissociation rate constants.

The spatial-temporal concentrations of the free target analyte ($[A](x, t)$), the free reporters ($[P](x,t)$), the analyte-reporter complex ($[PA](x,t)$, the test ligand-reporter complex at the capture (test) site ($[R_TP]$), the control ligand-analyte-reporter complex at the control site ($[R_CPA]$), and the control ligand-reporter complex at the control site ($[R_CP]$) are described, respectively, by the convection-diffusion-reaction equations:

$$\frac{\partial[A]}{\partial t} = D_A\frac{\partial^2[A]}{\partial x^2} - U\frac{\partial[A]}{\partial x} - F_{PA}, \quad (27)$$

$$\frac{\partial[P]}{\partial t} = D_P\frac{\partial^2[P]}{\partial x^2} - U\frac{\partial[P]}{\partial x} - F_{PA} - F_{RTP} - F_{RCP}, \quad (28)$$

$$\frac{\partial[PA]}{\partial t} = D_P\frac{\partial^2[PA]}{\partial x^2} - U\frac{\partial[PA]}{\partial x} + F_{PA} - F_{RCPA}, \quad (29)$$

$$\frac{\partial[R_TP]}{\partial t} = F_{RTP}, \quad (30)$$

$$\frac{\partial[RcP]}{\partial t} = F_{RCP}, \quad (31)$$

and

$$\frac{\partial[RcPA]}{\partial t} = F_{RCPA}. \quad (32)$$

The boundary conditions at $x=0$ are:

$$[A](0,t)=[A_e],\ [P](0,t)=[P_e],\ [PA](0,t)=[PA_e]. \quad (33)$$

At the membrane exit ($x=L$), as before, we specify the customary outflow conditions:

$$\frac{\partial [A](L,t)}{\partial x} = \frac{\partial [P](L,t)}{\partial x} = \frac{\partial [PA](L,t)}{\partial x} = 0 . \tag{34}$$

The initial conditions are:

$$[A](x,0)=[P](x,0)=[PA](x,0)=[R_TP](x,0)= [R_CPA](x,0)= [R_CP](x,0)=0. \tag{35}$$

F_{RTP} forms and $[R_TP]$ exists only in the capture (test) zone. Both are equal to zero elsewhere. Similarly, F_{RCPA} and F_{RCP} form and $[R_CPA]$ and $[R_CP]$ exist only at the control site and are equal to zero elsewhere.

Under well-mixed conditions, we have $[P]=[P_e]$, $[A]=[A_e]$, and $[PA]=[PA_e]$,

$$[R_T P] = \frac{k_{a2}[P][R_{T0}]}{k_{a2}[P] + k_{d2}} , \tag{36}$$

$$[R_C PA] = \frac{k_{a3}k_{d4}[PA][R_{C0}]}{k_{a3}k_{d4}[PA] + k_{d3}k_{a4}[P] + k_{d3}k_{d4}} , \tag{37}$$

and

$$[R_C P] = \frac{k_{d3}k_{a4}[P][R_{C0}]}{k_{a3}k_{d4}[PA] + k_{d3}k_{a4}[P] + k_{d3}k_{d4}} . \tag{38}$$

In the above, the analyte concentration $[A_0]$ does not appear explicitly. $[P_e]$ and $[PA_e]$ are, however, functions of $[A_0]$ (equations 20-22).

At low target analyte concentrations, equation 20 can be simplified, $[PA_e] \approx [A_0][P_0]\left([P_0] + \frac{k_{d1}}{k_{a1}}\right)^{-1}$, and $[P_e] \approx [P_0]\left(\frac{k_{a1}([P_0]-[A_0]) + k_{d1}}{k_{a1}[P_0] + k_{d1}}\right)$. The background signal $S_0=[P]+[PA]=[P_0]$, and the signals in the capture zone and at the control site are, respectively, $S_T= [P]+[PA]+[R_TP]=[P_0]+[R_TP]$ and $S_C=[P]+[PA]+[R_CPA]+[R_CP]=[P_0]+[R_CPA]+[R_CP]$. The contrast index $DS_T=[R_TP]/[P_0]$, and $DS_C=([R_CPA]+ [R_CP])/[P_0]$.

The signal level S_T-S_0 in the capture (test) zone is nearly constant when the target concentration is below the threshold $[A_{CT}]$. When $[A_0] << [A_{CT}]$,

$$\Delta S_T \sim \frac{k_{d2} + k_{a2}([P_0] + [R_{T0}])}{k_{d2} + k_{a2}[P_0]}[P_0]. \tag{39}$$

In the above,

$$[A_{CT}] = \frac{\{k_{d2} + k_{a2}([P_0] + [R_{T0}])\}(k_{d1} + k_{a1}[P_0])(k_{d2} + k_{a2}[P_0])}{k_{a1}k_{a2}k_{d2}[R_{T0}]}. \tag{40}$$

In other words, target analyte concentrations below the threshold $[A_{CT}]$ will not be detectable. Witness that the magnitude of the threshold depends on the reporter concentration and can be lowered by decreasing $[P_0]$.

When the target analyte concentration exceeds the threshold ($[A_{CT}]$), the signal's strength is inversely proportional to the concentration of the target analyte in the sample. When $[A_0] >> [A_{CT}]$,

$$\Delta S_T \sim \frac{k_{d2} + k_{a2}([P_0] + [R_{T0}])}{k_{d2} + k_{a2}[P_0]}[P_0] - \frac{k_{a1}k_{a2}k_{d2}[P_0][R_{T0}]}{(k_{d2} + k_{a2}[P_0])^2(k_{d1} + k_{a1}[P_0])}[A_0] \tag{41}$$

The signal level S_C-S_0 at the control site is nearly constant when the target concentration is below the threshold $[A_{CC}]$. When $[A_0] << [A_{CC}]$,

$$\Delta S_C \sim \frac{k_{d4} + k_{a4}([P_0] + [R_{C0}])}{k_{d4} + k_{a4}[P_0]}[P_0]. \tag{42}$$

In the above,

$$[A_{CC}] = \frac{k_{d3}\{k_{d4} + k_{a4}([P_0] + [R_{C0}])\}(k_{d1} + k_{a1}[P_0])(k_{d4} + k_{a4}[P_0])}{k_{a1}k_{d4}|k_{a3}k_{d4} - k_{a4}k_{d3}|[R_{C0}]}. \tag{43}$$

When $[A_0] >> [A_{CC}]$,

$$\Delta S_C \sim \frac{k_{d4} + k_{a4}([P_0] + [R_{C0}])}{k_{d4} + k_{a4}[P_0]}[P_0] + \frac{k_{a1}k_{d4}(k_{a3}k_{d4} - k_{a4}k_{d3})}{k_{d3}(k_{d1} + k_{a1}[P_0])(k_{d4} + k_{a4}[P_0])^2}[P_0][R_{C0}][A_0] \tag{44}$$

When $k_{a3}k_{d4}>k_{a4}k_{d3,}$ the signal's intensity at the control site increases as the concentration of the target analyte increases. When $k_{a3}k_{d4}<k_{a4}k_{d3,}$ the converse is true; the signal's intensity decreases as the target analyte concentration increases. When $k_{a3}k_{d4}=k_{a4}k_{d3,}$ S_C-S_0 is independent of the target analyte concentration.

Next, we examine the effect of the reporter concentration on the signal in the capture zone and at the control site. When the reporter concentration ($[P_0]$) is small,

$$\Delta S_T \sim \frac{k_{a1}k_{d2}[A_0]+k_{d1}(k_{d2}+k_{a2}[R_{T0}])}{k_{a1}k_{d2}[A_0]+k_{d1}k_{d2}}[P_0] \tag{45}$$

increases nearly linearly as the reporter concentration increases. However, as $[P_0]$ increases so does $[A_{CT}]$ (equation 40).

At the control site, when the reporter concentration ($[P_0]$) is small,

$$\Delta S_C \sim \frac{k_{a1}k_{d4}[A_0](k_{d3}+k_{a3}[R_{C0}])+k_{d1}k_{d3}(k_{d4}+k_{a4}[R_{C0}])}{k_{d3}k_{d4}(k_{a1}[A_0]+k_{d1})}[P_0] \tag{46}$$

increases nearly linearly as the reporter concentration increases.

3. RESULTS AND DISCUSSION

To illustrate the capabilities of the mathematical modeling, the convection-diffusion-reaction equations were solved numerically using the finite element package Femlab™. Unless otherwise stated, the results correspond to $k_{a1}=k_{a2}=10^6$ (1/MS), $k_{a3}=10^7$ (1/MS), $k_{d1}=k_{d2}=k_{d3}=10^{-3}$(1/s) in the **RPA** case; and $k_{a1}=k_{a2}=k_{a4}=10^6$ (1/MS), $k_{a3}=10^7$(1/MS), $k_{d1}=k_{d2}=k_{d3}=k_{d4}=10^{-3}$(1/s) in the **RPNA** case. $[P_0]=[R_{T0}]=[R_{C0}]=[A_0]$=10nM, L=0.04m, x_{L1}=L/2, x_{L2}=L/2+0.005, x_{C1}=3L/4, x_{C2}=3L/4+0.005. The reaction rate constants are consistent with the kinetics of the human interleukin-5 (the interaction between scIL5 and sIL5Rα) for which we have BIACORE data.

3.1 LF Detector with **RPA** Competitive Format: both target analytes and reporters bind to the test ligand.

Fig. 2 depicts the sequence of events when the analyte and reporters are pre-mixed prior to their introduction into the membrane. Since the reporters do not interact with the target analyte, the various species' concentrations in the sample remain unaltered until the sample's arrival in the capture (test) zone. We assume that a sufficient amount of analyte is available to eventually achieve equilibrium conditions in the capture (test) and control zones. The figure depicts the signal S as a function of the location x at various times t=2 (a), 3(b), 4(c), 5(d), 6(e), and 10(f) minutes in the absence ($[A_0]$=0, blue dashed line) and presence ($[A_0]$=10nM, red solid line) of target analyte. Away from the capture and control zones, $S=S_0=[P]$. In the capture (test) zone, $S=S_T=[P]+[R_TP]$. In the control zone, $S=S_C=[P]+[R_CP]$. Time $t=0$ corresponds to the instant when the solution starts flowing up the membrane. At time $t=2$ minutes (Fig. 2a), the solution has passed through the capture (test) site. Due to the interactions between the immobilized ligand and the reporters at the capture (test) and control sites, the concentration of the reporters at the capture (test) site (S_T) and at the control site (S_C) increases gradually over time until equilibrium conditions have been established. Once the sample arrives in the capture (test) zone (t>2min), upstream of the capture zone $S_0=[P_0]$. Since some of the reporters are retained in the interaction zones, initially the reporter concentration downstream of the interaction zones is smaller than upstream of the interaction zones. This downstream concentration increases, however, as time goes by, and once equilibrium conditions have been established, it is equal to the reporter concentration ($S_0=[P_0]$) upstream of the interaction zones. We refer to S_0 as the baseline. Once the equilibrium state has been reached, the signal contains

two peaks located at the capture (test) site and the control site. The amplitude of S_T-S_0 depends on rate constants $k_{a1,}$ k_{a2}, k_{d1}, and k_{d2}, and the concentrations of the test ligand [R_{T0}], target analyte [A_0] and reporter [P_0]. Witness that S_T is smaller in the presence of the target analyte (red line) than in its absence (blue line). Before equilibrium conditions have been established, the magnitude of S_C-S_0 depends on [A_0], the rate constants k_{a3} and $k_{d3,}$ and the concentrations [R_{C0}] and [P_0]. During the transient, the control signal is higher in the presence of the target analyte (red line) than in its absence (blue line). Once equilibrium has been reached, S_C is independent of [A_0].

Next, we examine the kinetics of the binding process. To this end, we calculate the average reporter concentration $\overline{S_T}(t) = \frac{1}{x_{L2} - x_{L1}} \int_{x_{L1}}^{x_{L2}} S_T(x,t)dx$ at the capture (test) site and $\overline{S_C}(t) = \frac{1}{x_{C2} - x_{C1}} \int_{x_{C1}}^{x_{C2}} S_C(x,t)dx$ at the control site. Fig. 3 depicts $\overline{S}_T(t)$ (solid line) and $\overline{S}_C(t)$ (dashed line) as functions of time for the same reaction constants as in Fig. 2 and various target analyte concentrations, [A_0]=0, 5, and 10nM. There is no signal before the sample arrives at the interaction zones. Once the sample has arrived at the interaction zones, the signal increases as time increases until it reaches a plateau that corresponds to the equilibrium state. Since the control zone is located downstream of the test zone, there is a time lag between the control and test signals. Fig. 3 illustrates that the lateral flow assay must be allowed sufficient time to "develop" before being read. The figure also shows the penalty associated with premature reading of the signal. The time required to reach the equilibrium state depends on the rate constants and the flow rate. As the target analyte concentration increases, the magnitude of the

test signal decreases. The magnitude of the equilibrium signal at the control site is independent of target analyte concentration.

Fig. 4 depicts $\Delta\overline{S}_T$ (solid blue line), $\Delta\overline{S}_C$ (dotted blue line), and the difference between the control signal and test signal $\overline{S}_C - \overline{S}_T$ (dash dotted black line) on a log-log scale as functions of the target analyte concentration ($[A_0]$) once equilibrium conditions have been established when $k_{a1}= k_{a2}= 10^6$ (1/MS), $k_{a3}= 10^7$ (1/MS), $k_{d1}=k_{d2}=k_{d3}=10^{-3}$ (1/s), $[P_0]$=10nM and $[R_{T0}]=[R_{C0}]$=10nM. Under equilibrium condition, solutions of the well mixed and the full mathematical models are same (comparisons are not shown here), and the results depicted in Fig.4 are obtained from the simple well-mixed model. Unfortunately, at low target analyte concentrations, the signal at the capture zone is relatively flat and insensitive to the analyte concentration. There is a concentration threshold or a critical target analyte concentration $[A_C]$ that must be exceeded before there is a noticeable effect on the test signal. The magnitude of the threshold target analyte concentration

$$[A_C] \approx \frac{k_{a2}k_{d1}[P_0] + k_{d1}k_{d2}}{k_{a1}k_{d2}} \tag{47}$$

depends both on the reaction rate constants and the initial reporter concentration ($[P_0]$). When the target analyte concentration increases above the threshold, the signal is inversely proportional to the target analyte's concentration. The dashed red line depicts the asymptotic behavior at large target analyte concentrations (equation 18). In contrast, when a sandwich assay is used and the target analyte concentration is relatively small, the signal increases nearly linearly with the analyte concentration.[16] The contrast index DS_T (not shown here) behaves similarly to the amplitude ΔS_T. At equilibrium, ΔS_C is independent of the target analyte concentration.

Fig. 4 also depicts the difference between the control signal and the test signal, $\overline{S}_C - \overline{S}_T$ (dash-dotted black curve), as a function of the target analyte concentration ($[A_0]$). The curve assumes a "S" shape, and it is bound from below and above with two horizontal asymptotes. When the target analyte concentration is very low, $\overline{S}_C - \overline{S}_T$ is nearly independent of $[A_0]$. When $[A_0]$ is larger than the critical concentration $[A_{C1}]$, $\overline{S}_C - \overline{S}_T$ increases as $[A_0]$ increases. As the target concentration increases further beyond a second critical value $[A_{C2}]$, $\overline{S}_C - \overline{S}_T$ saturates. This saturation is simply due to the fact that at high analyte concentrations, the test signal $\overline{S}_T \to [P_0]$, and $\overline{S}_C - \overline{S}_T \to \Delta S_C$, which is independent of $[A_0]$ as depicted in Fig.3. In the range $[A_{C1}]<[A_0]<[A_{C2}]$, one can estimate the target analyte concentration from the difference between the control and test signals.

The predictions in Fig. 4 are in qualitative agreement with experimental observations. Rigorous comparison with experiments was not possible due to a lack of information on the relevant reaction rate constants in the experiments. Instead, we compare relative quantities. Fig. 5 depicts the relative signal $\Delta\overline{S}_T / \Delta\overline{S}_{T\max}$ as a function of the relative target analyte concentration $[A_0]/[A_C]$. The solid line corresponds to our theoretical predictions with well-mixed model. The squares correspond to the experimental data taken from Fig. 3 in Ho and Waychope[18] (aflatoxin B_1, AFB_1, is the target analyte). The upright triangles correspond to the experimental data taken from Fig. 6 in Martorell et al.[19] (biotin is the target analyte), and the inverted triangles correspond to the experimental data taken from Fig.4B in Kim et al.[20] (MCLR is the target analyte). The predicted trends are consistent with the experimental data.

Fig. 6 depicts the equilibrium $\Delta\overline{S}_T$ as a function of the reporter concentration ($[P_0]$) and the test ligand concentration $[R_{T0}]$ on a log-log scale when $k_{a1}=k_{a2}=10^6$ (1/MS), $k_{a3}=10^7$ (1/MS),

and $k_{d1}=k_{d2}=k_{d3}=10^{-3}$ (1/s). At small $[P_0]$, $\Delta\overline{S}_T$ (red-dashed line, $[A_0]=[R_{T0}]=10$nM) increases nearly linearly as $[P_0]$ increases. Once a certain critical value ($[P_C]\sim\frac{k_{a1}k_{d1}[A_0]+k_{d1}k_{d2}}{k_{a2}k_{d1}}$) has been exceeded, $\Delta\overline{S}_T$ saturates and achieves a plateau. At relatively small reporter concentration, increasing the inventory of reporters increases the concentration of ligand-reporter complexes and contributes to the signal's magnitude. Once the critical reporter concentration has been exceeded, further increases in the concentration of the reporters do not add to the signal intensity and will have an adverse effect on the signal contrast.

Next, we examine the effect of the ligand concentration on the signal level ΔS_T under equilibrium conditions ($[P_0]=10$nM). The dashed blue and solid black lines (in Fig. 6) correspond, respectively to $[A_0]=10$nM and $[A_0]=1$nM. Not surprisingly, as $[R_{T0}]$ increases, so does the signal level. The predictions of Fig. 6 qualitatively agree with the experimental observations of Martorell et al.[19] In their experiments, the strips were coated with 1, 2.5 and 4.5μg of antibiotin (biotin is the target analyte). The strips with 1μg of antibiotin did not provide a visually discernible band. The response curves obtained using the strips containing 2.5 and 4.5μg of antibiotin had the same detection limit. A slight improvement in the working range was observed with the higher concentration of antibiotin on the strip. This is consistent with equation 17, which predicts the threshold $[A_C]$ to be independent of the ligands $[R_{T0}]$ concentration.

The results of figures 4 and 6 can be summarized in a three-dimensional plot. Fig. 7 depicts the equilibrium $\Delta\overline{S}_T$ as a function of $[A_0]$ and $[P_0]$ on a log-log scale when $k_{a1}=k_{a2}=10^6$ (1/MS), $k_{d1}=k_{d2}=10^{-3}$ (1/s) and $[R_{T0}]=10$nM. Witness that, consistent with equation 47, the critical target analyte concentration ($[A_C]$) increases, and the device's sensitivity decrease as the reporter concentration increases.

Fig. 8 depicts the equilibrium contrast index DS_T as a function of $[A_0]$ and $[P_0]$ on a log-log scale under the same conditions as Fig. 7. The contrast index decreases as the target analyte and reporter concentrations increase. Figs. 7 and 8 illustrate the trade off between signal intensity and signal contrast. One may have a high signal level and contrast level near $[P_C]$.

3.2 **RPNA** Format: target analytes bind to reporters but not to the test ligand

In this section, we discuss briefly the second competitive format in which the target analytes bind to the reporters rather than to the immobilized test ligand. There are many similarities between these two formats, but there are also some differences. In this section, we mention briefly the similarities and then focus mostly on the differences between the two formats.

The transients associated with the **RPNA** format are similar to the ones depicted in Fig. 2 and 3 and, in the interest of space, are not reproduced here. Figs. 9a and 9b depict, respectively, the test signal's level $\overline{S}_T - S_0$ and the control signal's level $\overline{S}_C - S_0$ as functions of the target analyte concentration under equilibrium conditions. When the target analyte concentration $[A_0]$ is smaller than the threshold concentration $[A_{CT}]$ (equation 40), the test signal's level $\overline{S}_T - S_0$ is nearly independent of $[A_0]$. When the target analyte concentration increases above the threshold, the signal decreases as the target analyte concentration increases. Fig. 9a resembles closely Fig. 4 (the test signal).

The behavior of the control signal in the **RPNA** format is generally different than that of the **RPA** format. $\overline{S}_C - S_0$ (Fig. 9b) in the **RPNA** format depends on the magnitude of the various reaction rate constants. When the target analyte concentration is small ($[A_0]<[A_{CC}]$ (equation 43), $\overline{S}_C - S_0$ is independent of $[A_0]$. Once the target analyte concentration increases above the

threshold value, $\overline{S}_C - S_0$ increases when $k_{a3}k_{d4}>k_{d3}k_{a4}$ (dashed line), remains the same when $k_{a3}k_{d4}=k_{d3}k_{a4}$ (solid line), and decreases when $k_{a3}k_{d4}<k_{d3}k_{a4}$ (dash-dot line). Once a second threshold value of $[A_0]$ is exceeded, the control signal saturates. Fig. 9b should be compared with Fig. 4 (the control signal). The behavior of the control signal of the **RPNA** format resembles that of the **RPA** format only when $k_{a3}k_{d4}=k_{d3}k_{a4}$.

The theoretical predictions of Fig. 9a agree qualitatively with the experimental data of Fig. 2 in Esch et al.[15] and Fig.5B in Niedbala et al.[17] Fig. 10 depicts the predicted and observed relative signals $\Delta\overline{S}_T / \Delta\overline{S}_{T\max}$ as functions of the relative target analyte concentration $[A_0]/[A_{CT}]$ (dashed red line and the symbols o and □). The dashed red line corresponds to our theoretical predictions with $k_{a1}=2\times10^5$(1/MS), $k_{a2}=k_{a4}=10^6$(1/MS), $k_{a1}=2\times10^6$(1/MS), $k_{d1}=k_{d2}=k_{d3}=k_{d4}=10^{-3}$(1/s), $[P_0]=[R_{T0}]=[R_{C0}]$=10nM. The circles (o) correspond to the experimental data taken from Fig. 2 in Esch et al.[15] and the hollow squares (□) correspond to experimental data taken from Fig. 5B in Niedbala et al.[17] (PCP is the target analyte). The theoretical predictions favorably agree with the experimental data.

Fig. 10 also compares the theoretical predictions of Fig. 9b with the experimental data from Fig.3 in Esch et al.[15] The figure depicts the predicted (solid blue line, $k_{a3}k_{d4}>k_{d3}k_{a4}$) and experimental (symbols ■) relative signal $\dfrac{\Delta\overline{S}_C - \Delta\overline{S}_{C\min}}{\Delta\overline{S}_{C\max} - \Delta\overline{S}_{C\min}}$ as a function of the relative target analyte concentration $[A_0]/[A_{CM}]$. $[A_{CM}]$ is defined below. The blue curve in Fig. 10 is S-shaped. In other words, the curve has a lower (y^-) and an upper (y^+) horizontal asymptote. Let $[A^+]$ and $[A^-]$ be the respective concentrations at which the curve approaches the upper and lower asymptotes within $0.01(y^+-y^-)$. We define the concentration $[A_{CM}]$ as the geometric mean of $[A^+]$ and $[A^-]$, $[A_{CM}]=([A^+][A^-])^{1/2}$. Witness the good agreement between experiment and theory.

In the capture zone, the signal's amplitude $\overline{S}_T - S_0$ and the contrast index DS_T, expressed as functions of $[A_0]$ and $[P_0]$, behave similarly to the **RPA** case (Figs. 7-8). In the interest of space, the corresponding figures are not reproduced here. The behavior of the control signal in the **RPNA** case differs, however, from the **RPA** case.

Figs. 11 and 12 depict, respectively, the equilibrium control signal amplitude ($\Delta\overline{S}_C$) and the control signal contrast index DS_C as functions of $[A_0]$ and $[P_0]$ when $k_{a3}k_{d4}>k_{d3}k_{a4}$. As long as the reporter concentration is below a certain threshold ($[P_{CC}]$), the control signal increases as the reporter concentration increases, where $[P_{CC}] = \dfrac{k_{d2}[R_{T0}](k_{a1}[A_0]+k_{d1})}{k_{a1}k_{d2}[A_0]+k_{d1}(k_{a2}[R_{T0}]+k_{d2})}$. Once this threshold value has been exceeded, the signal levels off. At a fixed reporter concentration, the curve corresponding to the control signal as a function of the target analyte concentration has a "S" shape. The upper curve in Fig. 9b is a cross-section of the three-dimensional surface at a fixed reporter concentration. Fig. 12 illustrates that increases in the reporter concentration do not come without a penalty. As the reporter concentration increases, the control signal contrast decreases.

Figs. 13 and 14 depict, respectively, the control signal amplitude ($\Delta\overline{S}_C$) and the control signal contrast as functions of $[A_0]$ and $[P_0]$ when $k_{a3}k_{d4}<k_{d3}k_{a4}$ and under equilibrium conditions. As in Fig. 11, as long as the reporter concentration is below a certain threshold ($[P_{CC}]$), the control signal increases as the reporter concentration increases. The lower curve of Fig. 9b represents a cross-section of the surface in Fig. 13 at a fixed reporter concentration. Like Fig. 12, Fig. 14 demonstrates that as the reporter concentration increases, the contrast index decreases.

When $k_{a3}k_{d4} \neq k_{d3}k_{a4}$ the target analyte concentration affects both the test and control signals in the **RPNA** format. Thus, one can determine the presence of the target in the sample based on both signals.

Fig. 15 depicts the difference between the equilibrium control signal and the equilibrium test signal, $\overline{S}_C - \overline{S}_T$, as function of $[A_0]$ and $[P_0]$ when $k_{a3}k_{d4} > k_{d3}k_{a4}$. For a specified reporter concentration, $\overline{S}_C - \overline{S}_T$ increases as the target analyte concentration increases. Once the target analyte concentration exceeds a certain threshold, the curve saturates. As the reporter concentration increases from zero, the signal difference increases (from zero), attains a maximum, and then decreases again. Similar phenomena are observed when $k_{a3}k_{d4} < k_{d3}k_{a4}$ and $k_{a3}k_{d4} = k_{d3}k_{a4}$.

4. Conclusions

Mathematical models for competitive Lateral Flow (LF) assays are proposed. The models allow one to predict the test and control signals' magnitudes as functions of the target analyte and reporter concentrations as well as the various reaction constants. The models' predictions agree qualitatively with experimental observations.

Unfortunately, quantitative comparison between theory and experiment was hindered by the lack of data about the reaction rate constants of the various interacting species and, in particular, the lack of information about the interaction kinetics between analytes in solution and particle-bound ligands and between particles in solution and ligands immobilized to the lateral flow strip. In the future, we hope to conduct experiments to measure the reaction rate constants needed to carry out a critical comparison between the experiments and theory.

The main observations are:

(i) When the target analyte concentration is below a certain threshold value, the test signal is nearly independent of the analyte concentration. In order to be able to detect the presence of target analytes, the analyte concentration must exceed the threshold value. The threshold's magnitude depends on the reaction rate constants and the concentration of the reporters. Hence, it is possible to adjust the LF detector's sensitivity by adjusting the concentration of the reporters.

(ii) Above the target analyte threshold value, the test signal's intensity is inversely proportional to the target analyte concentration.

(iii) At low reporter concentrations, the signal level increases as the reporter concentration increases. Once a certain threshold reporter concentration has been exceeded, the signal saturates.

(iv) At low reporter concentrations, the contrast index is independent of the reporter concentration. Once a threshold has been exceeded, the contrast index decreases as the reporter concentration increases.

(v) In **RPA** format and equilibrium conditions, the control signal's level is independent of the target analyte concentration. In contrast, in the **RPNA** format, depending on the relative magnitudes of the various reaction rate constants, the control signal may either decrease, remain unchanged, or increase as the target analyte concentration increases.

We hope that the proposed models will be useful for the design of LF reactors operating with competitive assays. The models can also be used to test inexpensively and rapidly device performance under various operating conditions. Although the simulations cannot substitute

for experiments, they can help narrow the experimental parameter space.

ACKNOWLEDGMENTS

The work described in this paper was supported, in part, by DARPA's SIMBIOSYS program (Dr. Anantha Krishnan, program director) and by NIH grant 1U01 DE 14964-01. We are grateful to Professor P. Corstjens (Leiden University), Professor D. Malamud and Dr. Z. Chen (University of Pennsylvania), and Dr. J. Graden (OraSure Technologies, Inc.) for useful discussions.

REFERENCES

[1] C. Barrett, C. Good, C. Moore, Comparison of point-of-collection screening of drugs of abuse in oral fluid with a laboratory-based urine screen, Forensic Science International, 122 (2001) 163-166

[2] A. Jehanli, S. Brannan, L. Moore, V.R. Spiehler, Blind trials of an onsite saliva drug test for marijuana and opiates, Journal of Forensic Sciences, 46 (2001) 1214-1220

[3] Y. Oku, K. Kamiya, H. Kamiya,Y. Shibahara, T. Ii, Y. Uesaka, Development of oligonucleotide lateral-flow immunoassay for multi-parameter detection, Journal of Immunological Methods, 258 (2001) 73-84

[4] M. Lonnberg, J. Carlsson, Quantitaive Detection in the Attomole Range for Immunochromatographic tests by Means of a Flatbed Scanner, Analytical Biochemistry, 293(2001) 224-231

[5] H.L. Smits, C.K.Eapen, S. Sugathan, M. Kuriakose, M.H. Gasem, C.Yersin, D. Sasaki, B. Pujianto, M. Vestering, T.H. Abdoel, G.C. Gussenhoven, Lateral-flow assay for rapid serodiagnosis of human leptospirosis, Clinical and Diagnostic Laboratory Immunology, 8 (2001) 166-169

[6] F. Ketema, C. Zeh, D.C. Edelman, R. Saville, N.T. Constantine, Assessment of the performance of a rapid, lateral flow assay for the detection of antibodies to HIV, Journal of Acquirer Immune Deficiency Syndromes, 27 (2001) 63-70

[7] F.E. Ahmed, Detection of genetically modified organisms in foods, Trends in Biotechnology, 20 (2002) 215-223

[8] Y. Al-Yousif, J. Anderson, C. Chard-Bergstrom, S. Kapil, Development, evaluation, and application of lateral-flow immunoassay (immunochromatography) for detection of rotavirus in bovine fecal samples, Clinical and Diagnostic Laboratory Immunology, 9 (2002) 723-724

[9] C. Quach, D. Newby, G. Daoust, E. Rubin, J. McDonald, QuickVue influenza test for rapid detection of influenza A and B viruses in a pediatric population, Clinical and Diagnostic Laboratory Immunology, 9 (2002) 925-926

[10] J. Tao, N. DelosSantos, C. Dou, One step lateral flow immunoassay for detection of Ecstasy in human urine, Clinical Chemistry, 48 (2002) B14 Part 2

[11] A. Salomone, P. Roggero, Host range, seed transmission and detection by ELISA and lateral flow of an Italian isolate of Pepino mosaic virus, Journal of Plant Pathology, 84 (2002) 65-68

[12] P. Corstjens, M. Zuiderwijk, M. Nilsson, H. Feindt, R. S. Niedbala, H. J.Tanke, Lateral-Flow and Up-Converting Phosphor Reporters to Detect Single-Stranded Nucleic Acids in Sandwich-Hybridization Assay, Analytical Biochemistry, 312(2003)191-200

[13] P. Corstjens , M. Zuiderwijk, A. Brink, S. Li, H. Feindt, R.S. Neidbala, H. Tanke, Use of up-converting phosphor reporters in lateral-flow assays to detect specific nucleic acid sequences: A rapid, sensitive DNA test to identify human papillomavirus type 16 infection,

Clinical Chemistry, 47 (2001) 1885-1893

[14] S.P. Johnston, M.M. Ballard, M.J. Beach, L. Causer, P.P. Wilkins, Evaluation of three commercial assays for detection of giardia and cryptosporidium organisms in fecal specimens, Journal of Clinical Microbiology, 41 (2003) 623-626

[15] M.B. Esch, A.J. Baeumner, R.A. Durst, Detection of Cryptosporidium parvum using oligonucleotide-tagged liposomes in a competitive assay format, Analytical Chemistry, 73 (2001), 3162-3167.

[16] S. Qian, H.H. Bau, A mathematical model of lateral flow bio-reactions applied to sandwich assays, Analytical Biochemistry, 2003, in press

[17] R.S. Niedbala, H. Feindt, K. Kardos, T. Vail, J. Burton, B. Bielska, S. Li, D. Milunic, P. Bourdelle, R.Vallejo, Detection of analytes by immunoassay using up-converting phosphor technology, Analytical Biochemistry, 293 (2001) 22-30

[18] J.A.A. Ho, R.D.Wauchope, A strip liposome immunoassay for aflatoxin B-1, Analytical Chemistry, 74(2002), 1493-1496.

[19] D. Martorell, S.T.A. Siebert, R.A. Durst, Liposome dehydration on nitrocellulose and its application in a biotin immunoassay *Analytical Biochemistry*, 271(1999), 177-185.

[20] Y.M. Kim, S.W. Oh, S.Y. Jeong, D.J. Pyo, E.Y. Choi, Development of an ultrarapid one-step fluorescence immunochromatographic assay system for the quantification of microcystins, Environmental Science and Technology, 37(2003),1899-1904.

[21] W.K. Fong, Z. Modrusan, J.P. McNevin, J. Marostenmaki, B. Zin, F. Bekkaoui, Rapid solid-phase immunoassay for detection of methicillin-resistant Staphylococcus aureus using cycling probe technology, Journal of Clinical Microbiology, 38 (2000) 2525-2529

[22] M. Lonnberg, J. Carlsson, Chromatographic performance of a thin microporous bed of nitrocellulose, Journal of Chromatography B-Analytical Technologies in the Biomedical and Life Sciences, 763 (2001) 107-120

[23] H.H. Weetall, K.R. Rogers, A simple assay for 2,4-dichlorophenoxyacetic acid using coated test-strips, Analytical Letters, 35 (2002) 1341-1348

[24] J. Hampl, M. Hall, N.A. Mufti, Y.M. Yao, D.B. MacQueen, W. H. Wright, D.E. Cooper, Upconverting Phosphor Reporters in Immunochromatographic Assays, Analytical Biochemistry,288(2001)176-187

Lists of Captions:

1. A schematic diagram of the lateral flow bio-detector with a competitive assay format. A mixture of target analyte *A* and reporter particles *P* migrates by capillary force up the membrane towards the test and control sites.
2. The signal S as a function of the spatial coordinate x at various times t=2(a), 3(b), 4(c), 5(d), 6(e), and 10(f) min with **RPA** format. $k_{a1}=k_{a2}=10^6$ (1/MS), $ka_3=10^7$(1/MS), $k_{d1}= k_{d2}=k_{d3}=10^{-3}$(1/s), $[P_0]= [R_{T0}]= [R_{C0}]$=10nM. The red solid line and the blue dashed line correspond, respectively, to $[A_0]$=10nM and 0nM.
3. The averaged test ($\overline{S}_T$ solid lines) and control ($\overline{S}_C$ dashed lines) signals as functions of time at various target analyte concentrations $[A_0]$= 0, 5, and 10nM. **RPA** format. $k_{a1}=k_{a2}=10^6$ (1/MS), $ka_3=10^7$(1/MS), $k_{d1}= k_{d2}=k_{d3}=10^{-3}$(1/s), and $[P_0]= [R_{T0}]= [R_{C0}]$=10nM.
4. The test signal ($\overline{S}_T$-S_0, blue solid line), the control signal ($\overline{S}_C$-S_0, blue dotted line), and the difference between the control and test signals ($\overline{S}_C$-$\overline{S}_T$, black dashed line) as functions of the target analyte concentration under equilibrium conditions. **RPA** format. $k_{a1}=k_{a2}=10^6$ (1/MS), $ka_3=10^7$(1/MS), $k_{d1}= k_{d2}=k_{d3}=10^{-3}$(1/s), and $[P_0]= [R_{T0}]= [R_{C0}]$=10nM.
5. The normalized signal as a function of the normalized target analyte concentration $[A_0]/[A_C]$. The solid line corresponds to the equilibrium predictions. The symbols (□), (Δ) and (∇) correspond, respectively, to experimental data from Fig.3 in Ho and Waychope[18], experimental data from Fig.6 in Martorell et al.[19], and experimental data from Fig.4B in Kim et al.[20]

6. The signal's equilibrium amplitude $\overline{S}_T$-S_0 is depicted as a function of the reporter concentration (red dashed line) when $[A_0]=[R_{T0}]=10nM$ and as a function of the concentration of immobilized test ligand (black solid line, $[A_0]=1nM$, and blue dashed line, $[A_0]=10nM$) when $[P_0]=10nM$. **RPA** format. $k_{a1}=k_{a2}=10^6$ (1/MS), $ka_3=10^7$(1/MS), and $k_{d1}= k_{d2}=k_{d3}=10^{-3}$(1/s).

7. The test signal's equilibrium amplitude ($\overline{S}_T$-S_0) as a function of the target analyte concentration $[A_0]$ and the reporter concentration $[P_0]$. **RPA** format. $k_{a1}=k_{a2}=10^6$ (1/MS), $ka_3=10^7$(1/MS), $k_{d1}= k_{d2}=k_{d3}=10^{-3}$(1/s), and $[R_{T0}]= [R_{C0}]=10nM$.

8. The test signal's equilibrium contrast DS_T as a function of the target analyte concentration $[A_0]$ and the reporter concentration $[P_0]$. **RPA** format. $k_{a1}=k_{a2}=10^6$ (1/MS), $ka_3=10^7$(1/MS), $k_{d1}= k_{d2}=k_{d3}=10^{-3}$(1/s), and $[R_{T0}]= [R_{C0}]=10nM$.

9. The test ($\overline{S}_T$-S_0, a) and control ($\overline{S}_C$-S_0, b) signals' amplitudes as functions of the target analyte concentration under equilibrium conditions. **RPNA** format. $k_{a1}=k_{a2}=k_{a4}=10^6$ (1/MS), $k_{d1}= k_{d2}=k_{d3}=k_{d4}=10^{-3}$(1/s), and $[P_0]= [R_{T0}]= [R_{C0}]=10nM$. The dash line, solid line, and dash dot line in (b) correspond, respectively to $ka_3=10^7$(1/MS), 10^6(1/MS), and 10^5(1/MS).

10. The normalized test signal as a function of the normalized target analyte concentration $[A_0]/[A_{CT}]$ (dashed red line and symbols o and □), and the normalized control signal as a function of the normalized analyte target concentration $[A_0]/[A_{CM}]$ (solid blue line and symbols ■). **RPNA** format. The solid and dashed lines correspond to the equilibrium predictions with $k_{a1}=2\times10^5$(1/MS), $k_{a2}=k_{a4}=10^6$(1/MS), $k_{a1}=2\times10^6$(1/MS), $k_{d1}=k_{d2}=k_{d3}=k_{d4}=10^{-3}$(1/s), and $[P_0]= [R_{T0}]= [R_{C0}]=10nM$. The symbols (o) and (■) correspond, respectively, to the experimental data from Fig.2 and

Fig.3 in Esch et al.[15]. The symbols (□) correspond to the experimental data from Fig.5B in Niedbala et al.[17].

11. The control signal's amplitude $\overline{S}_C$-S_0 as a function of the target analyte concentration $[A_0]$ and the reporter concentration $[P_0]$. **RPNA** format. $k_{a1}=k_{a2}=k_{a4}=10^6$ (1/MS), $ka_3=10^7$(1/MS), $k_{d1}= k_{d2}=k_{d3}=k_{d4}=10^{-3}$(1/s), and $[R_{T0}]= [R_{C0}]$=10nM.
12. The control signal's contrast index DS_C as a function of the target analyte concentration $[A_0]$ and the reporter concentration $[P_0]$. **RPNA** format. $k_{a1}=k_{a2}=k_{a4}=10^6$ (1/MS), $ka_3=10^7$(1/MS), $k_{d1}= k_{d2}=k_{d3}=k_{d4}=10^{-3}$(1/s), and $[R_{T0}]= [R_{C0}]$=10nM.
13. The control signal's amplitude $\overline{S}_C$-S_0 as a function of the target analyte concentration $[A_0]$ and the reporter concentration $[P_0]$. **RPNA** format. $k_{a1}=k_{a2}=k_{a4}=10^6$ (1/MS), $ka_3=10^5$(1/MS), $k_{d1}= k_{d2}=k_{d3}=k_{d4}=10^{-3}$(1/s), and $[R_{T0}]= [R_{C0}]$=10nM.
14. The control signal's contrast index DS_C as a function of the target analyte concentration $[A_0]$ and the reporter concentration $[P_0]$. **RPNA** format. $k_{a1}=k_{a2}=k_{a4}=10^6$ (1/MS), $ka_3=10^5$(1/MS), $k_{d1}= k_{d2}=k_{d3}=k_{d4}=10^{-3}$(1/s), and $[R_{T0}]= [R_{C0}]$=10nM.
15. The difference between the control signal $\overline{S}_C$ and the test signal $\overline{S}_T$ as a function of the target analyte concentration $[A_0]$ and the reporter concentration $[P_0]$. **RPNA** format. $k_{a1}=k_{a2}=k_{a4}=10^6$ (1/MS), $ka_3=10^7$(1/MS), $k_{d1}= k_{d2}=k_{d3}=k_{d4}=10^{-3}$(1/s), and $[R_{T0}]= [R_{C0}]$=10nM.

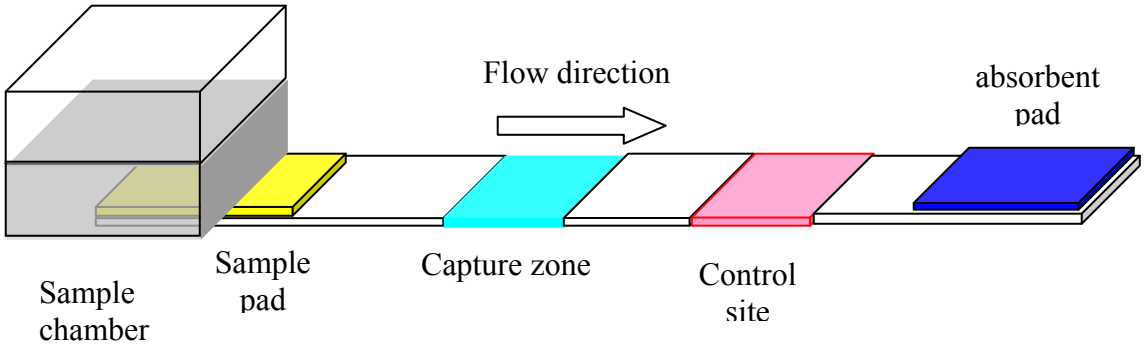

Fig.1: A schematic diagram of the lateral flow bio-detector with a competitive assay format. A mixture of target analyte *A* and reporter particles *P* migrates by capillary force up the membrane towards the test and control sites.

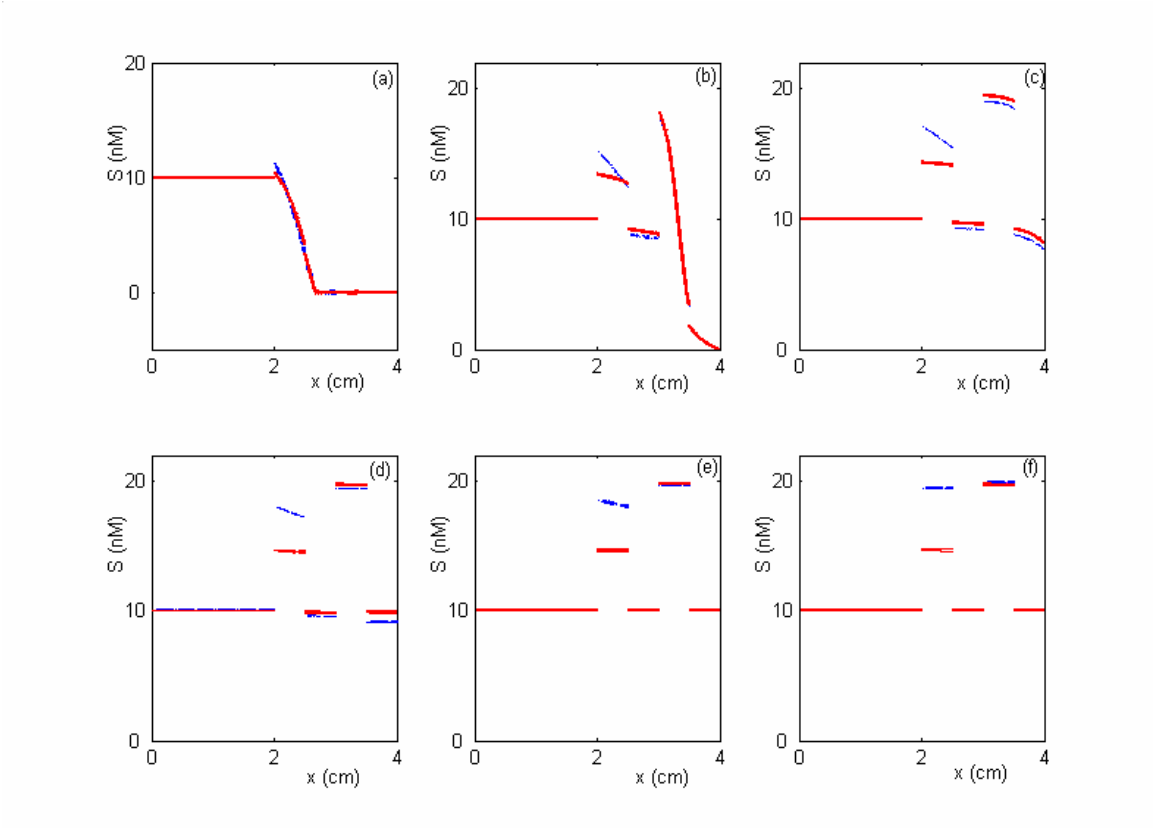

Fig. 2: The signal S as a function of the spatial coordinate x at various times t=2(a), 3(b), 4(c), 5(d), 6(e), and 10(f) min with **RPA** format. $k_{a1}=k_{a2}=10^{6}$ (1/MS), $ka_3=10^{7}$(1/MS), $k_{d1}=k_{d2}=k_{d3}=10^{-3}$(1/s), $[P_0]=[R_{T0}]=[R_{C0}]=10$nM. The red solid line and the blue dashed line correspond, respectively, to $[A_0]=10$nM and 0nM.

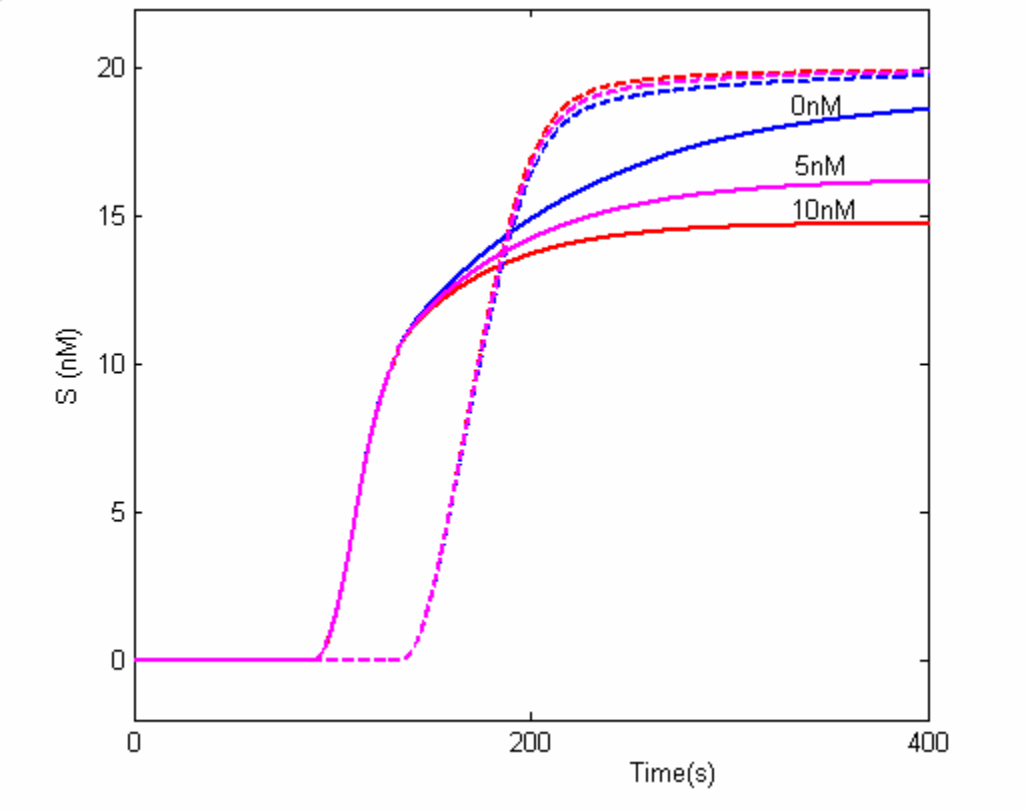

Fig.3: The averaged test ($\overline{S}_T$ solid lines) and control ($\overline{S}_C$ dashed lines) signals as functions of time at various target analyte concentrations [A_0]= 0, 5, and 10nM. **RPA** format. $k_{a1}=k_{a2}=10^6$ (1/MS), $ka_3=10^7$(1/MS), $k_{d1}= k_{d2}=k_{d3}=10^{-3}$(1/s), and [$P_0$]= [$R_{T0}$]= [$R_{C0}$]=10nM.

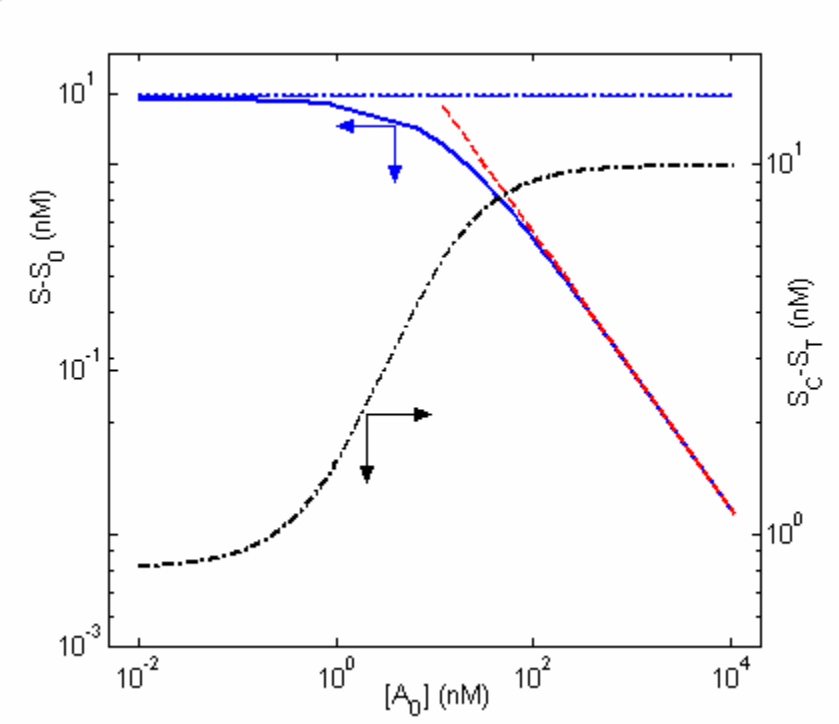

Fig.4: The test signal ($\overline{S}_T$-S_0, blue solid line), the control signal ($\overline{S}_C$-S_0, blue dotted line), and the difference between the control and test signals ($\overline{S}_C$-$\overline{S}_T$, black dashed line) as functions of the target analyte concentration under equilibrium conditions. **RPA** format. $k_{a1}=k_{a2}=10^6$ (1/MS), $ka_3=10^7$(1/MS), $k_{d1}=k_{d2}=k_{d3}=10^{-3}$(1/s), and $[P_0]=[R_{T0}]=[R_{C0}]$=10nM.

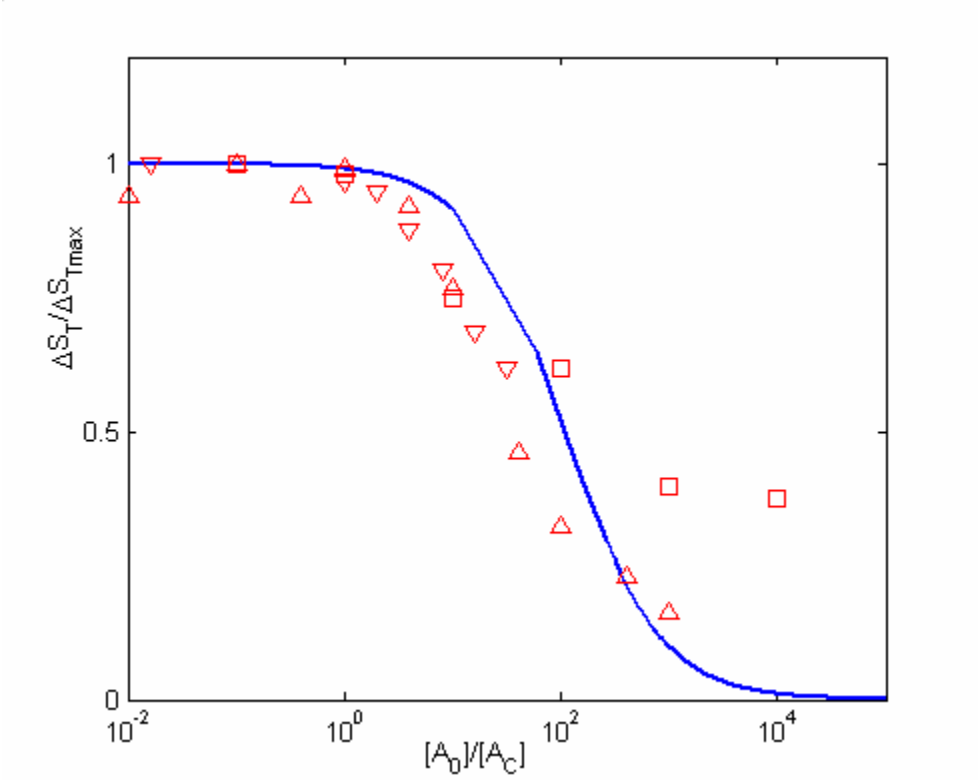

Fig.5: The normalized signal as a function of the normalized target analyte concentration $[A_0]/[A_C]$. The solid line corresponds to the equilibrium predictions. The symbols (□), (Δ) and (∇) correspond, respectively, to experimental data from Fig.3 in Ho and Waychope[18], experimental data from Fig.6 in Martorell et al.[19], and experimental data from Fig.4B in Kim et al.[20]

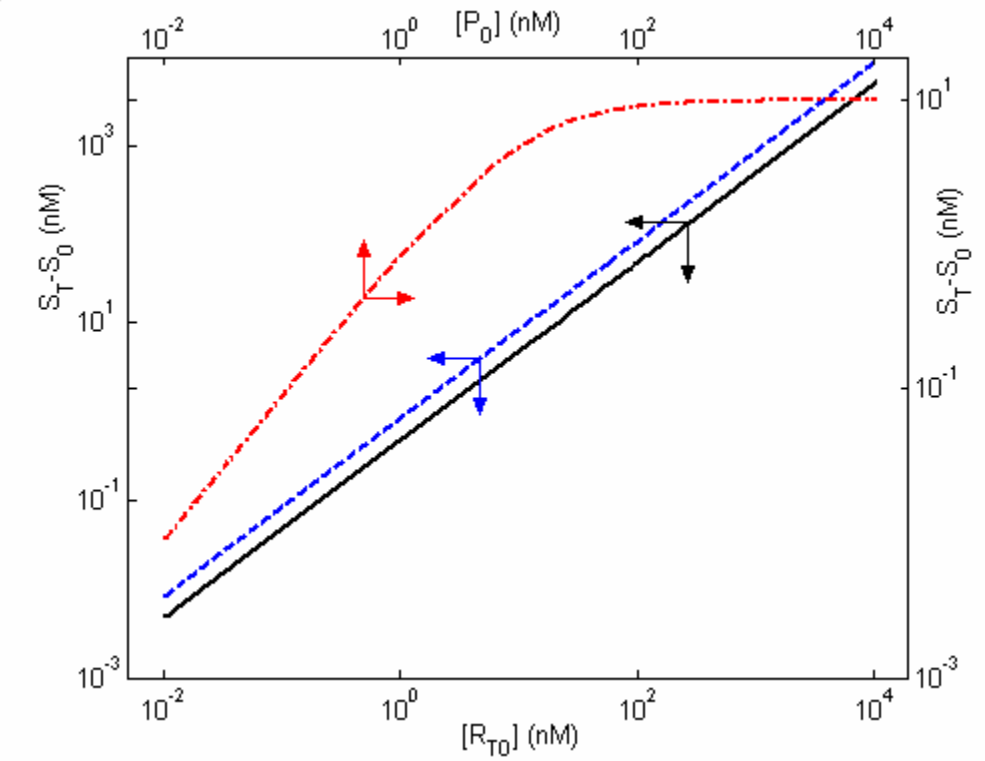

Fig. 6: The signal's equilibrium amplitude $\overline{S}_T$-S_0 is depicted as a function of the reporter concentration (red dashed line) when $[A_0]=[R_{T0}]=10$nM and as a function of the concentration of immobilized test ligand (black solid line, $[A_0]=1$nM, and blue dashed line, $[A_0]=10$nM) when $[P_0]=10$nM. **RPA** format. $k_{a1}=k_{a2}=10^6$ (1/MS), $ka_3=10^7$(1/MS), and $k_{d1}= k_{d2}=k_{d3}=10^{-3}$(1/s)..

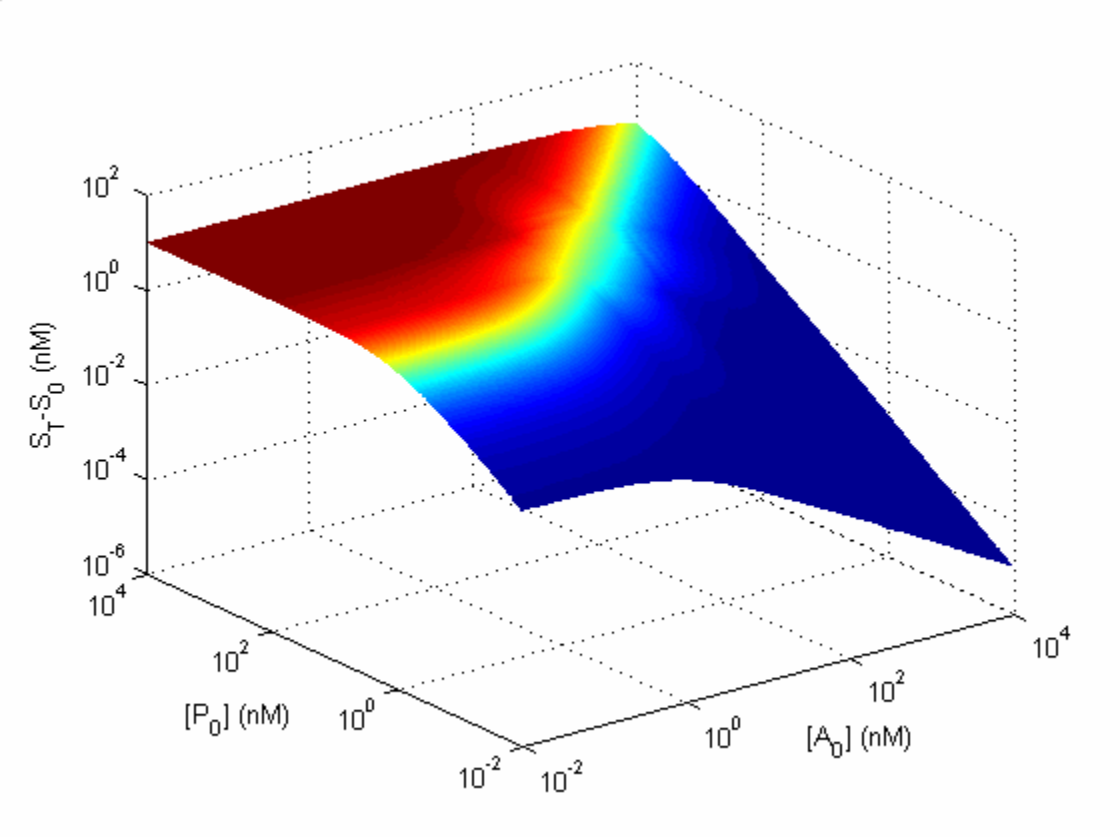

Fig.7: The test signal's equilibrium amplitude ($\overline{S}_T$-S_0) as a function of the target analyte concentration [A_0] and the reporter concentration [P_0]. **RPA** format. $k_{a1}=k_{a2}=10^6$ (1/MS), $ka_3=10^7$(1/MS), $k_{d1}= k_{d2}=k_{d3}=10^{-3}$(1/s), and $[R_{T0}]= [R_{C0}]=10$nM.

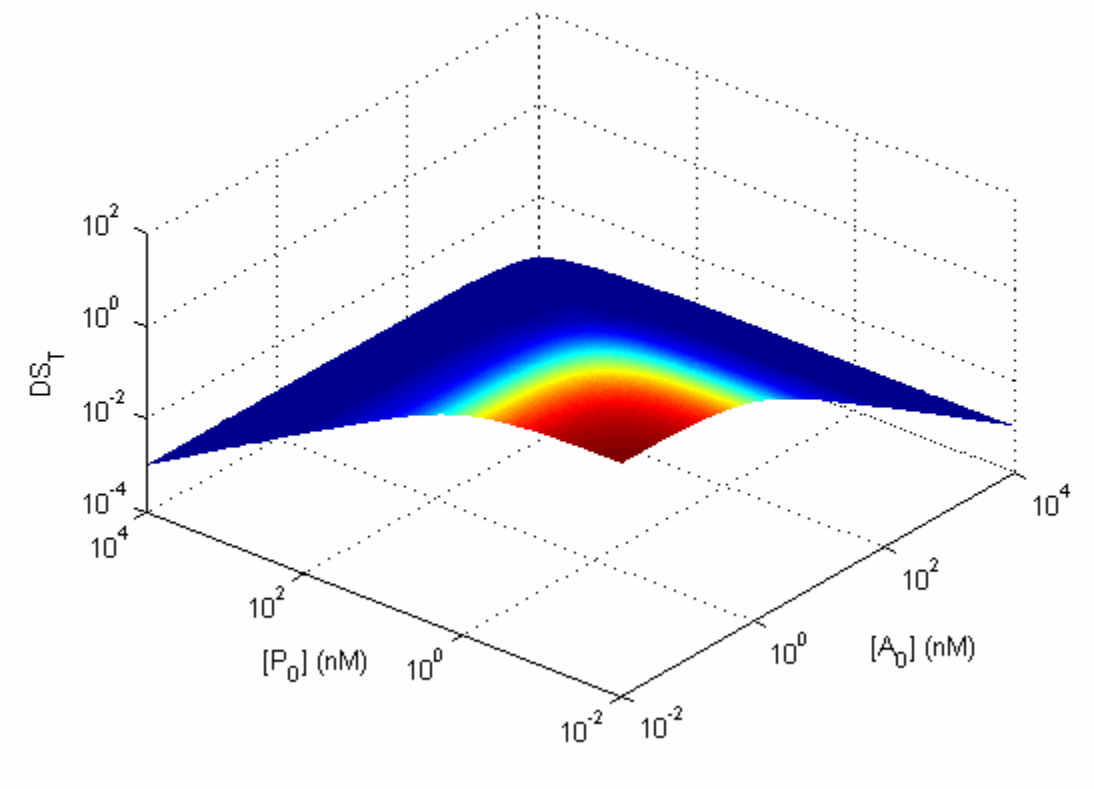

Fig.8: The test signal's equilibrium contrast DS_T as a function of the target analyte concentration $[A_0]$ and the reporter concentration $[P_0]$. **RPA** format. $k_{a1}=k_{a2}=10^6$ (1/MS), $ka_3=10^7$(1/MS), $k_{d1}= k_{d2}=k_{d3}=10^{-3}$(1/s), and $[R_{T0}]= [R_{C0}]$=10nM.

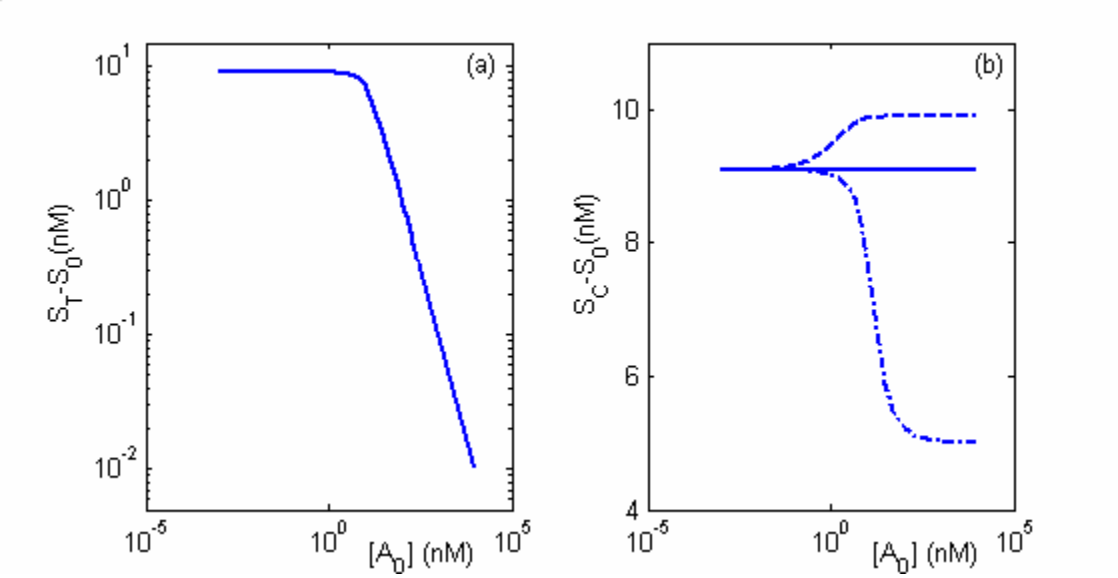

Fig.9: The test ($\overline{S}_T$-S_0, a) and control ($\overline{S}_C$-S_0, b) signals' amplitudes as functions of the target analyte concentration under equilibrium conditions. **RPNA** format. $k_{a1}=k_{a2}=k_{a4}=10^6$ (1/MS), $k_{d1}= k_{d2}=k_{d3}=k_{d4}=10^{-3}$(1/s), and $[P_0]= [R_{T0}]= [R_{C0}]$=10nM. The dash line, solid line, and dash dot line in (b) correspond, respectively to $ka_3=10^7$(1/MS), 10^6(1/MS), and 10^5(1/MS).

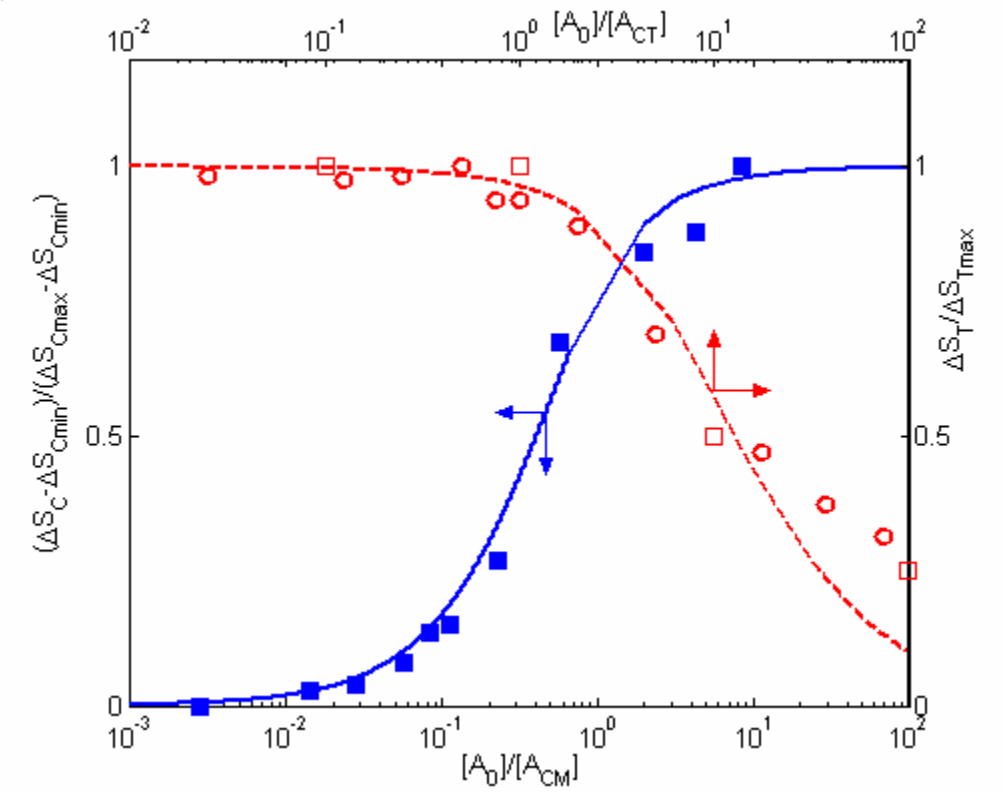

Fig.10: The normalized test signal as a function of the normalized target analyte concentration $[A_0]/[A_{CT}]$ (dashed red line and symbols o and □), and the normalized control signal as a function of the normalized analyte target concentration $[A_0]/[A_{CM}]$ (solid blue line and symbols ■). **RPNA** format. The solid and dashed lines correspond to the equilibrium predictions with $k_{a1}=2\times10^5$(1/MS), $k_{a2}=k_{a4}=10^6$(1/MS), $k_{a1}=2\times10^6$(1/MS), $k_{d1}=k_{d2}=k_{d3}=k_{d4}=10^{-3}$(1/s), and $[P_0]=[R_{T0}]=[R_{C0}]$=10nM. The symbols (o) and (■) correspond, respectively, to the experimental data from Fig.2 and Fig.3 in Esch et al.[15]. The symbols (□) correspond to the experimental data from Fig.5B in Niedbala et al.[17].

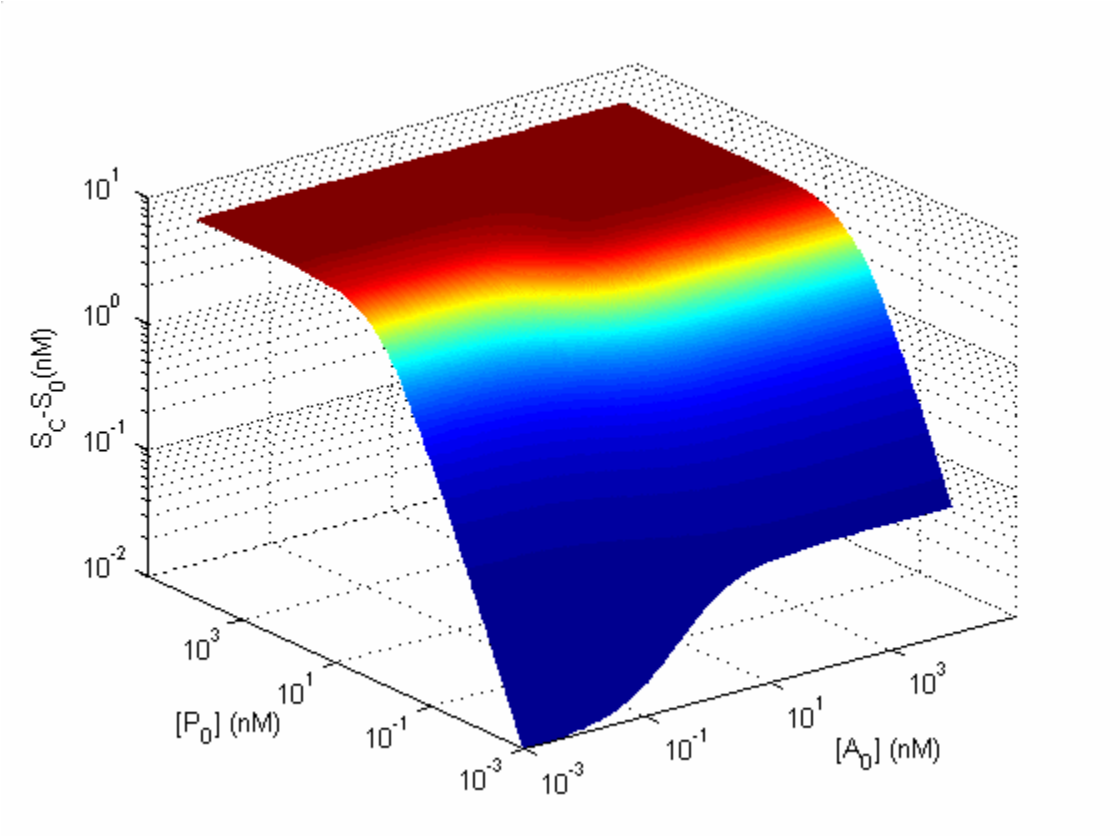

Fig.11: The control signal's amplitude $\overline{S}_C$-S_0 as a function of the target analyte concentration $[A_0]$ and the reporter concentration $[P_0]$. **RPNA** format. $k_{a1}=k_{a2}=k_{a4}=10^6$ (1/MS), $ka_3=10^7$(1/MS), $k_{d1}= k_{d2}=k_{d3}=k_{d4}=10^{-3}$(1/s), and $[R_{T0}]= [R_{C0}]$=10nM.

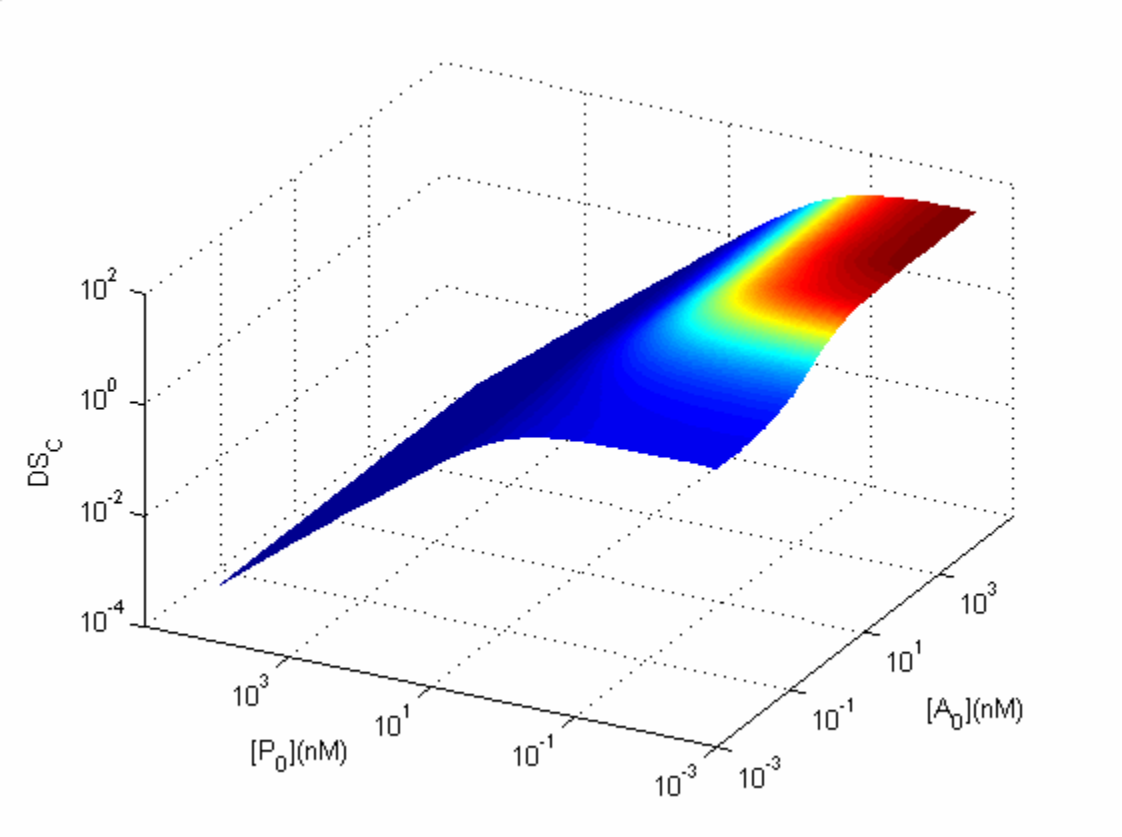

Fig.12: The control signal's contrast index DS_C as a function of the target analyte concentration $[A_0]$ and the reporter concentration $[P_0]$. **RPNA** format. $k_{a1}=k_{a2}=k_{a4}=10^{6}$ (1/MS), $ka_3=10^{7}$(1/MS), $k_{d1}= k_{d2}=k_{d3}=k_{d4}=10^{-3}$(1/s), and $[R_{T0}]= [R_{C0}]=10$nM.

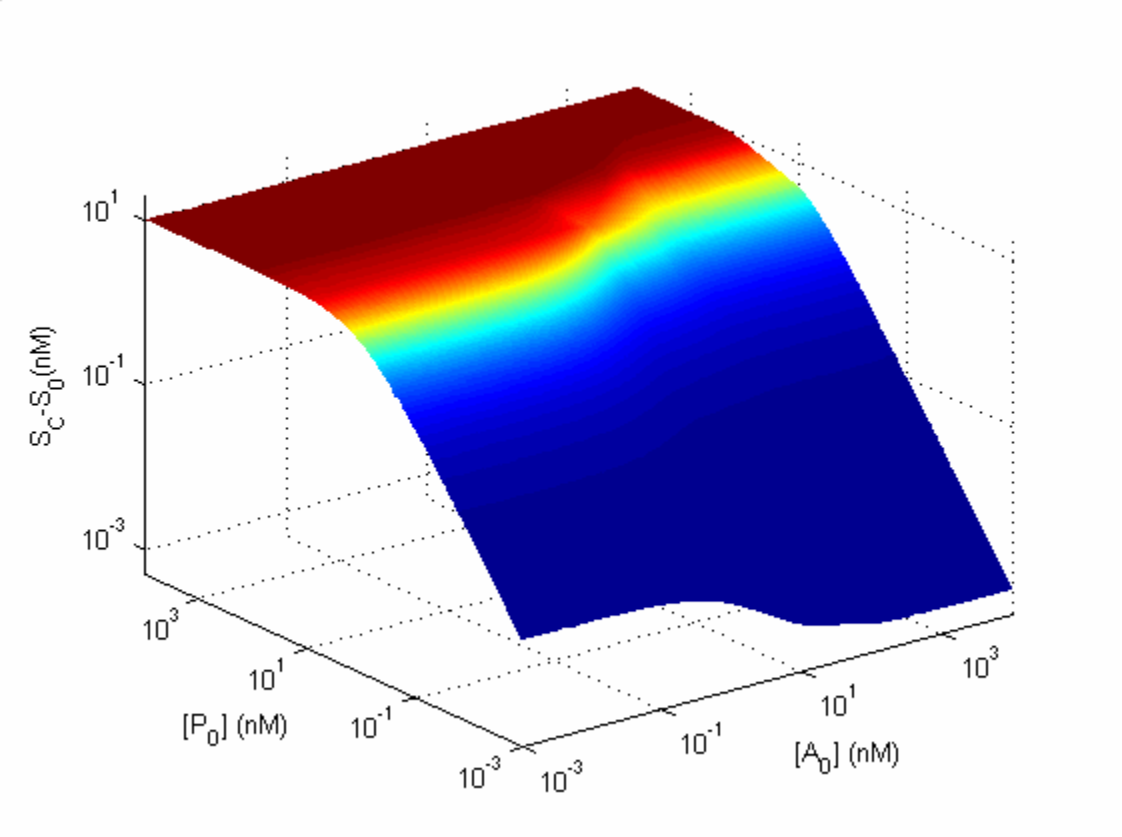

Fig.13: The control signal's amplitude $\overline{S}_C$-S_0 as a function of the target analyte concentration [A_0] and the reporter concentration [P_0]. **RPNA** format. $k_{a1}=k_{a2}=k_{a4}=10^6$ (1/MS), $ka_3=10^5$(1/MS), $k_{d1}= k_{d2}=k_{d3}=k_{d4}=10^{-3}$(1/s), and $[R_{T0}]= [R_{C0}]$=10nM.

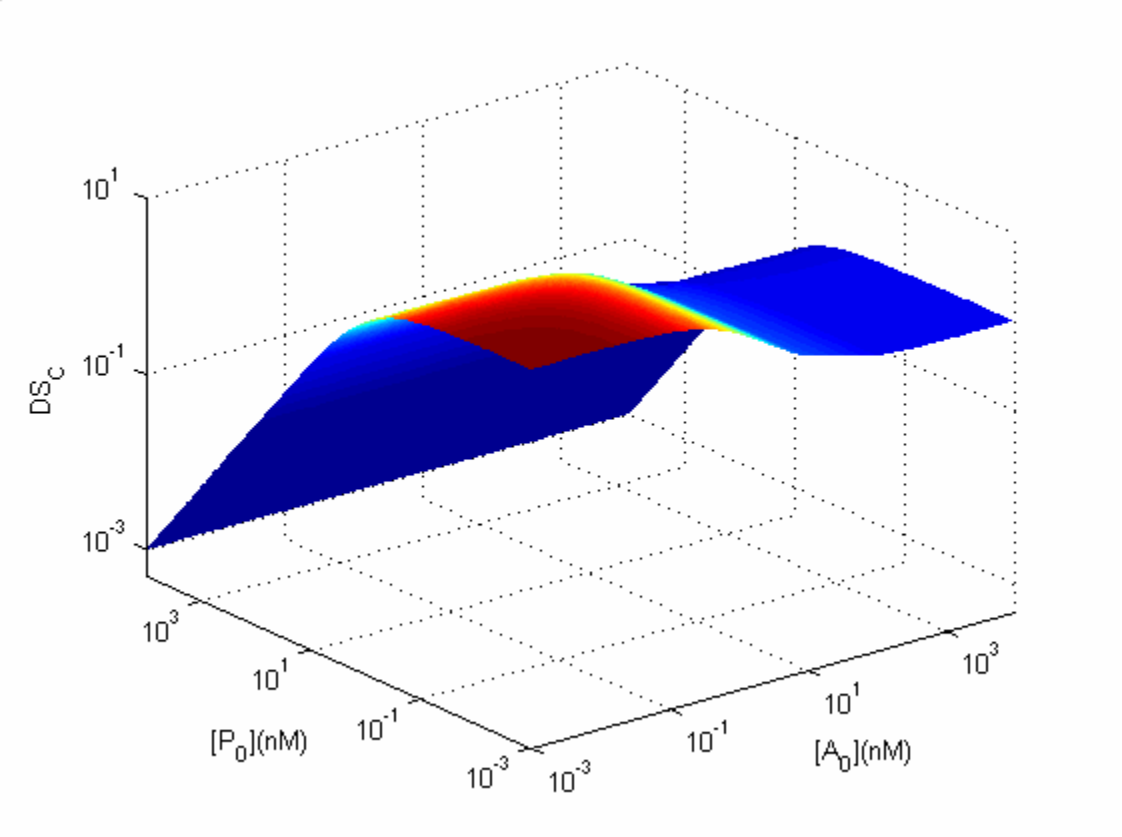

Fig.14: The control signal's contrast index DS_C as a function of the target analyte concentration $[A_0]$ and the reporter concentration $[P_0]$. **RPNA** format. $k_{a1}=k_{a2}=k_{a4}=10^6$ (1/MS), $ka_3=10^5$(1/MS), $k_{d1}= k_{d2}=k_{d3}=k_{d4}=10^{-3}$(1/s), and $[R_{T0}]= [R_{C0}]$=10nM.

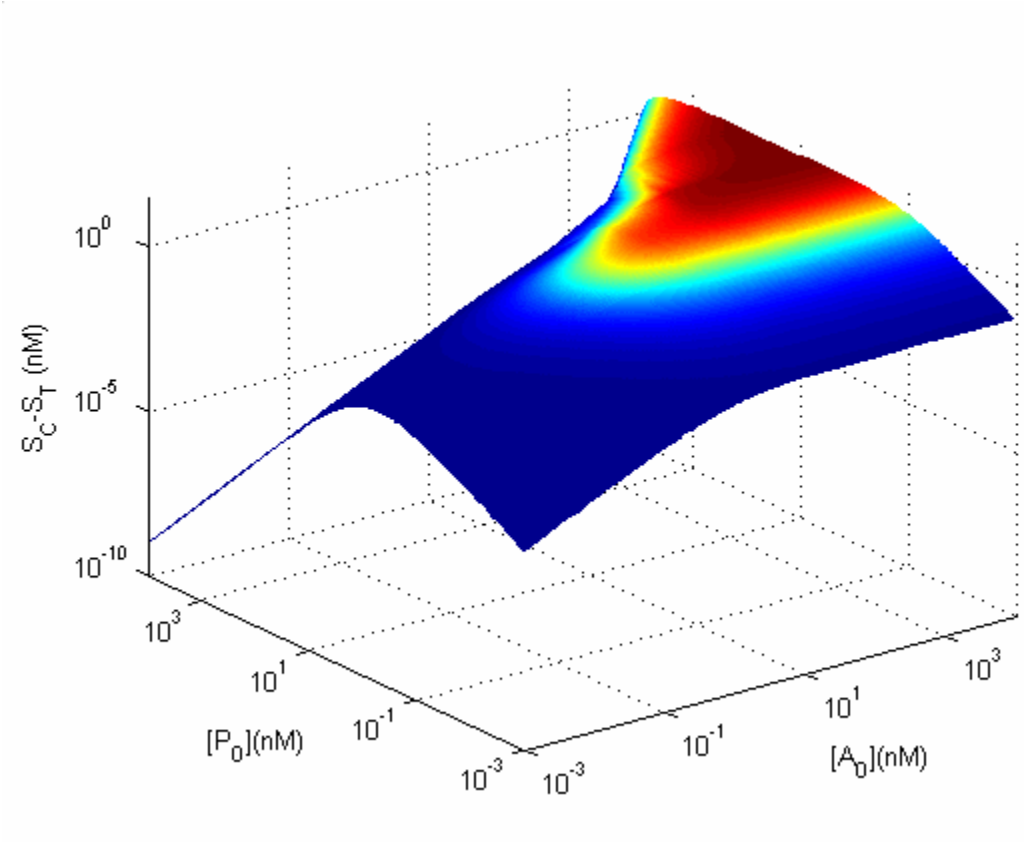

Fig.15: The difference between the control signal $\bar{S}_C$ and the test signal $\bar{S}_T$ as a function of the target analyte concentration [A_0] and the reporter concentration [P_0]. **RPNA** format. $k_{a1}=k_{a2}=k_{a4}=10^6$ (1/MS), $ka_3=10^7$(1/MS), $k_{d1}= k_{d2}=k_{d3}=k_{d4}=10^{-3}$(1/s), and $[R_{T0}]=[R_{C0}]$=10nM.